Journal of Physics D: Applied Physics

TOPICAL REVIEW

Molecular polymer-derived ceramics for applications in electrochemical energy storage devices

To cite this article: Santanu Mukherjee *et al* 2018 *J. Phys. D: Appl. Phys.* **51** 463001

IOP Publishing Journal of Physics D: Applied Physics
J. Phys. D: Appl. Phys. **51** (2018) 463001 (19pp) https://doi.org/10.1088/1361-6463/aadb18

Topical Review

Molecular polymer-derived ceramics for applications in electrochemical energy storage devices

Santanu Mukherjee[1], **Zhongkan Ren and Gurpreet Singh**[1]

Department of Mechanical and Nuclear Engineering, Kansas State University, KS 66506, United States of America

E-mail: santanum@ksu.edu and gurpreet@ksu.edu

Received 19 April 2018, revised 29 June 2018
Accepted for publication 17 August 2018
Published 7 September 2018

Abstract

Development of efficient electrochemical energy storage systems with high energy and power densities coupled with minimal carbon footprint is an important technological challenge. One vital aspect in this regard is the correct choice of electrode material, as its properties (chemical, electrical) and assorted aspects (availability, processability) strongly influence the performance of the electrochemical system. Significant research has gone into developing novel electrode materials for the various electrochemical systems (Li-ion and other metal-ion rechargeable batteries, supercapacitors, etc); however, in most cases, it is hard to identify a single electrode material that works suitably well across all systems. Molecular precursor or polymer derived ceramics (PDCs), because of their amorphous nanodomain structure, processing flexibility, easy availability of precursors, and tunable electrochemical properties, are promising candidates as electrode materials for a range of electrochemical energy storage devices. With progressive research, as more information is garnered about the relationship between PDC molecular structure and electrochemical behavior, it is expected that PDC-based materials will make a significant impact on the development of the next generation of high capacity, energy efficient batteries and supercapacitors. This article therefore looks to provide a detailed discussion of the properties of PDCs and their status as energy storage materials, along with the challenges that lie ahead.

Keywords: polymer-derived ceramics, silicon, pyrolysis, lithium ion batteries, supercapacitors, anode

(Some figures may appear in colour only in the online journal)

1. Introduction

With the realization of fossil fuel's negative impact on the environment, rechargeable electrochemical energy storage devices are being considered as a way out of this important energy challenge facing modern civilization (Bruce *et al* 2008, Goodenough and Park 2013). Rechargeable metal-ion batteries, since Sony Corporation™ introduced the first commercial 'rocking-chair' type Li-ion battery (LIB) in 1991, have revolutionized electrochemical energy storage and have provided significant improvements in telecommunications, portable electronics, automobiles and even grid storage (Barré *et al* 2013, Goodenough and Park 2013, Slater *et al* 2013, Blomgren 2017). Currently, not only LIBs, but also sodium ion batteries (SIBs) are receiving significant research attention because of their inherent advantages: extensive availability of

[1] Author to whom any correspondence should be addressed

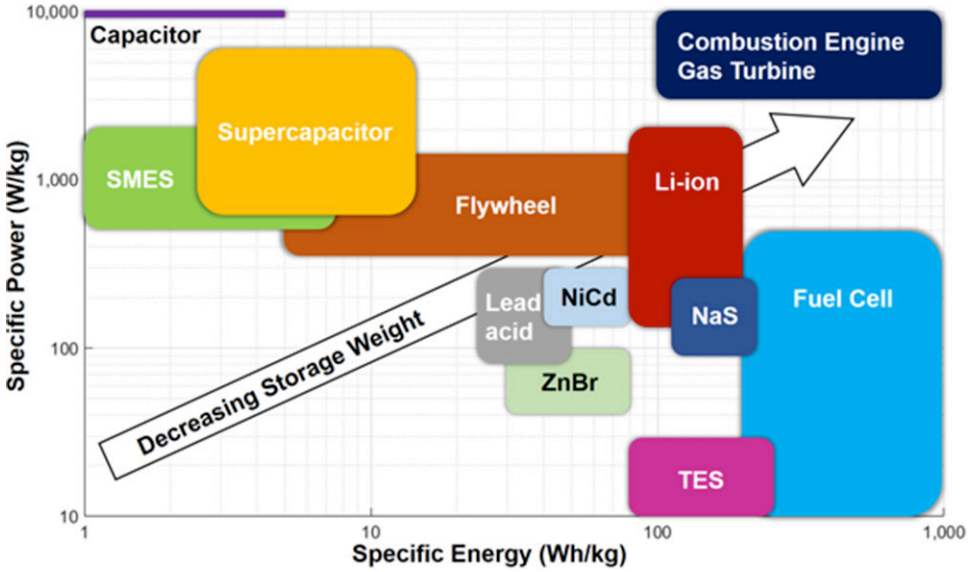

Figure 1. Comparison of various energy storage systems. Comparison of specific power and energy of the LIB with other commonly used commercial batteries. Reproduced from (Luo *et al* 2015). CC BY 3.0.

Na metal in the earth's crust, lower establishment and manufacturing cost, usability for large scale grid storage, potential for use with less toxic, flammable and even aqueous electrolytes, etc (Ellis and Nazar 2012, Yabuuchi *et al* 2014).

However, emerging metal ion rechargeable batteries pose their own characteristic set of challenges, especially with respect to their design and choice of electrode and electrolyte materials: flammability, structural degradation of electrodes, inability to accommodate large sized alkali ions, etc, are major challenges, and are discussed in greater detail in the following section. Energy and power density of various types of electrochemical energy storage systems including Li-ion batteries and supercapacitors are compared with traditional energy storage systems such as the flywheel and combustion engine in figure 1.

PDC materials, ever since their large scale introduction in the 1960s, have demonstrated novel physical and chemical properties including their high specific surface area and ability to cycle lithium ions at room temperature, which makes them a potential candidate for use in electrochemical devices (Colombo *et al* 2010). Also, a large variation in properties of the ceramic is possible by altering their processing parameters, as well as composition of pre-ceramic polymer, which has allowed PDCs to be studied as high power density electrode materials for Li-ion batteries (Bhandavat *et al* 2012b).

2. Issues in current electrochemical energy storage devices

Electrochemical energy storage can be considered a reasonably mature science, with significant global commercialization and research activity (Jiang *et al* 2012, Chen and Xue 2016). However, it is important to realize that current electrochemical storage devices suffer from several important issues which must be addressed if their full potential is to be realized.

For LIBs, some of the issues can be discussed as follows.

Electrode decomposition is one of the most important factors that limits the usability of rechargeable metal ion batteries. Batteries usually function within the oxidative range of the electrolyte, and if this range is sometimes exceeded, dissolution of the positive electrode occurs, resulting in reduced cell lifetimes (Scrosati and Garche 2010). Similarly, continuous charging and discharging results in undesirable side reactions at both the anode and the cathode side, causing quicker electrode degradation (Scrosati and Garche 2010, Yuan *et al* 2017). These processes lead to progressive capacity fading as well, as the integrity of the electrode structure is irreversibly lost (Yuan *et al* 2017).

Formation of a solid–electrolyte interface layer is a significant drawback frequently encountered (An *et al* 2016). Intercalation of alkali metal ions generally results in the formation of a solid–electrolyte interface (SEI) at the electrode surface, resulting in consumption of some of those ions (An *et al* 2016, Yu *et al* 2017). This is an irreversible process, especially in the first few cycles of battery performance. SEI, however, can be considered a necessary evil, as it helps to stabilize the cell after the initial few cycles and prevents further electrode degradation (Yu and Manthiram 2018). Coulombic efficiency is defined as the ratio of amount of charge stored during discharge to that of the amount delivered during the previous charging cycle (Smith *et al* 2010). Multiple causes such as unwanted side reactions, electrode degradation, formation of passivating layers, etc, result in significant reduction in coulombic efficiency, as well as capacity fading, with progressive cycling of the cell (Xua *et al* 2015).

Operational safety is another important consideration that must be kept in mind for LIBs. The electrolytes used in the case of LIBs are toxic, flammable and sometimes prone to explosion (Arbizzani *et al* 2011, Scrosati *et al* 2011). Formation of dendrites—especially if Li metal is used as the anode—is an important safety issue, as these dendrites eventually lead to short-circuiting of the cell and this raises another concern: potential explosion (Bhattacharyya *et al* 2010). Therefore, battery design and proper heat removal systems are essential in the proper functioning of LIBs. **Non-LIBs**, especially SIBs,

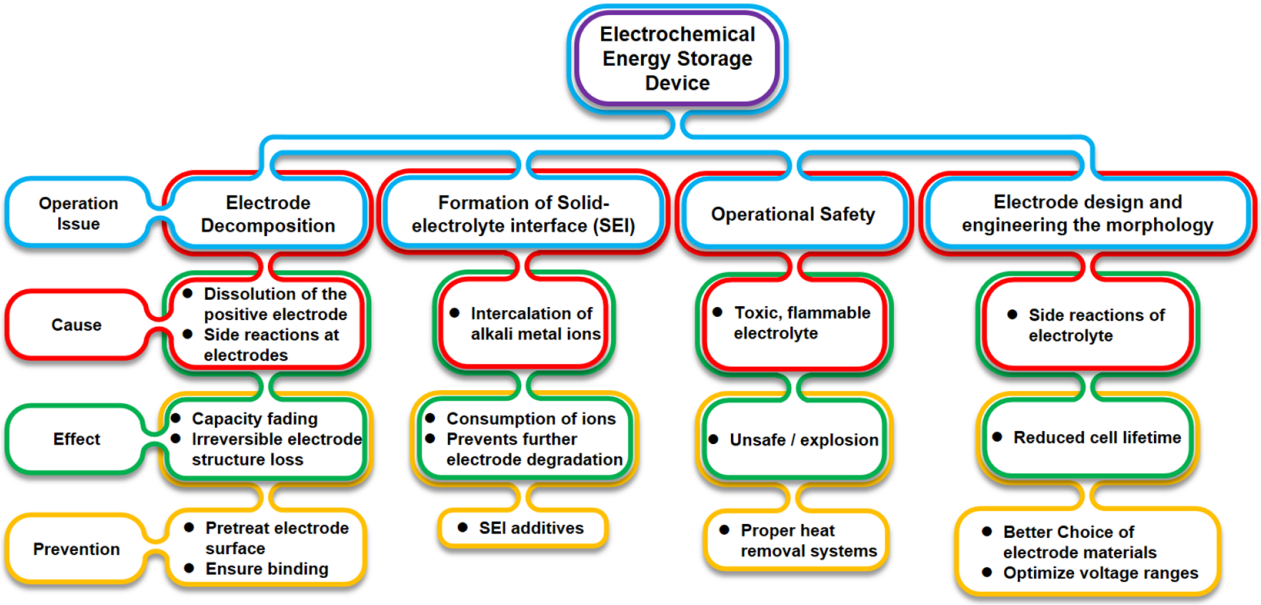

Figure 2. Issues faced by energy storage system electrodes. Flowchart depicting the various issues faced by electrochemical energy storage systems and how these manifest themselves, along with steps that can be taken to overcome them and improve performance. Reproduced with permission from (Bhandavat *et al* 2012b).

pose a different set of challenges which are unique to themselves, apart from the issues mentioned above.

The *large size* of the Na^+ ion places considerable constraints on the types of electrode that can be used (Sawicki and Shaw 2015). Graphite, a commonly used negative electrode in LIBs, cannot be used with SIBs as it does not provide sufficient interlayer spacing to accommodate Na^+ ions (Slater *et al* 2013, Sawicki and Shaw 2015). Similarly, when pure metals or metal alloys are used as the electrode, there is a danger of structural degradation and pulverization because of the large volume changes due to intercalation/alloying of large sized Na^+ ions (Sawicki and Shaw 2015, Mukherjee *et al* 2017). Sn or Sb compounds and alloys are especially susceptible to this sort of damage (Baggetto *et al* 2014).

Electrode design and engineering of morphology is an especially important factor in case of non-LIBs. Na metal is very reactive and tends to form long slender structures called dendrites which grow progressively with undesirable side reactions (Stevens and Dahn 2000). These dendrites have the ability to grow from one electrode to another, thereby ultimately shorting the cell and seriously reducing its working lifetime (Stevens and Dahn 2000). Electrode materials must be chosen and run within voltage ranges such that this issue can be minimized. Also, the inherent capacities and energy densities in SIBs are lower due to the sluggish kinetics of the large sized Na^+ ions, and so open structured electrodes, which allow for easy reversible intercalation, must be preferred (Kundu *et al* 2015).

The challenges faced by supercapacitors are similar to those facing the previously mentioned battery systems. Similarly to batteries, the components needed in supercapacitors—e.g. the electrodes, electrolyte and separator—need to be compatible with each other for smooth performance. Capacity fading is an important issue, as is the cost of manufacture (Hsieh *et al* 2008). In addition, maintaining stability of the electrolyte over large number of cycles (generally 20000 or more cycles) is another issue that is frequently encountered. For aqueous-electrolyte-based supercapacitors, the voltage range is limited to ~1.2 V, which significantly reduces the available energy density (Zhao and Zheng 2015).

These factors indicate that prudent choice of the electrode material is imperative to overcome many of the issues faced. This provides the rationale for the use of PDCs as electrode materials for LIBs and non-LIBs. A further detailed analysis of the properties of PDCs and what makes them superior as energy storage materials is discussed in the following section.

A schematic representation of the various issues, their causes and effects and the ways that these issues can be mitigated is provided in figure 2.

3. Polymer-derived ceramic (PDC) systems and a discussion of their important properties

PDCs have gained extensive attention due to their excellent properties such as high mechanical strength (Young's modulus of 150 ± 10 GPa, Vickers hardness of 25 GPa–27 GPa), elevated electrical conductivity (6×10^{-3} S cm^{-1}), remarkable thermostability, resistance to corrosive environment and creep (Colombo *et al* 2001, Shah and Raj 2002). Also, the final properties of the PDCs can be very effectively modified by tailoring the processing parameters, and this is what makes PDCs so desirable (Greil 1998).

The microstructure of PDCs essentially resembles a network of atoms similar in structure to graphene, with a network of sp_2 bonded carbon atoms located at the boundary of tetrahedral nanodomains of silica (Riedel *et al* 2006). This is caused primarily by the limited solubility of carbon in silica. Increasing demand for superior properties of ceramics and

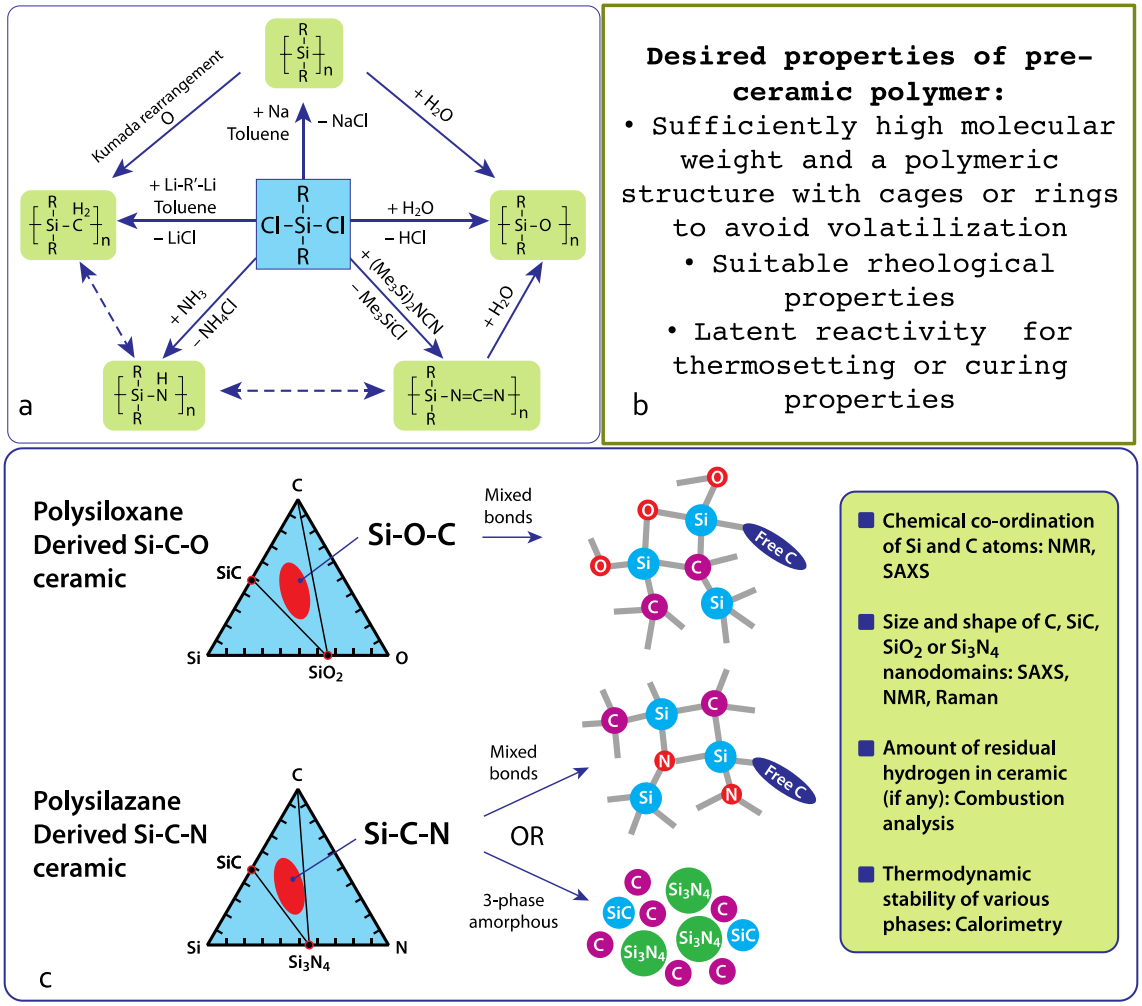

Figure 3. Structural property relations of the SiOC and SiCN systems. (a) Chloro-organosilicon compounds (generally by-products of the silicone industry) are low-cost precursors to pre-ceramic polymers. Reproduced from (Ionescu *et al* 2012) with permission of The Royal Society of Chemistry. (b) Manufacturing of PDC ceramic fibers requires certain desired characteristics such as suitable rheological properties and latent reactivity. (c) Composition diagrams of polymer-derived SiOC and SiCN ceramics and schematic showing predicted corresponding atomic arrangements. The presence of nanodomains (e.g. SiC, SiO_2 or Si_3N_4, C) in PDCs is an intriguing feature of these materials. Reproduced from (Mera *et al* 2013) with permission of The Royal Society of Chemistry. Because the ceramics are x-ray amorphous, structural characterization requires advanced techniques such as SAXS, EXELFS, XPS and NMR. *Note: composition diagrams of other B and Al doped PDCs are more complex and not shown here.*

rising challenges in engineering have accelerated the advancement of research and development in PDCs (Riedel *et al* 2006, Bernard and Miele 2014). Under these circumstances, recent analysis has shown several functional properties of PDCs to be eligible for application in electrochemical energy storage devices (Saha and Raj 2006, Stormer *et al* 2007, Morcos *et al* 2008, Mera *et al* 2009). Figures 3(a) and (b) provide a schematic representation of the range of precursors and reaction paths that can be used to develop the requisite pre-ceramic polymers, along with their relevant properties. Figure 3(c) is a schematic of the types of bond found in SiOC and SiCN PDCs.

Several important properties of PDCs, especially those important regarding electrochemical energy storage devices, are discussed briefly below.

3.1. Chemical and thermodynamic stability

Chemical and thermodynamic stability is an important criterion for a good electrode material. The electrode in a battery/supercapacitor is often subjected to corrosive environments, and should be able to resist degradation in these regimes.

Chemical stability is a function of the bond strength of the different constituent elements in the PDC. Compared to conventional crystalline Si_3N_4 or SiC, polymer-derived SiCN exhibits greater chemical stability owing to the existence of securely bonded Si–C and a lack of long term order in the ceramic structure (Kleebe *et al* 2001, Yu and Raj 2015b). Nucleophilic reactions are prevented by the Si–C bond; additionally, the layered carbon network, which resembles graphene, largely suppresses the diffusion of chemicals into these ceramics (Soraru and Modena 2002).

Thermodynamically, PDCs with ternary systems (such as SiCN or SiOC) exhibit better stability than those with binary systems of the same elements, such as SiC, SiO_2 and Si_3N_4 (Ionescu *et al* 2012). The graphene network of insoluble free carbon formed at the silicon tetrahedral interdomain reduces the mobility of atoms, resulting in limited crystallization even at high temperatures (Saha and Raj 2006). With regards to

composition of PDCs, higher carbon content generally leads to a more amorphous structure. For example, in SiOC based PDCs, the free C phase prevents quick crystallization by hindering the mobility of atoms whereas in SiCN systems, the graphene analogous network of C atoms forms a net-like structure around the Si_3N_4 nanodomains, thereby limiting nitrogen diffusion (Mera *et al* 2013). Crystallization and decomposition resistance at a high temperature can also be enhanced by incorporation of elements such as B, Hf and Zr (Guron *et al* 2008). Thermal stability of SiBCN ceramic is again improved from its parent SiCN, since the doping of boron creates turbostratic structure of B–C–N phase that further reduces diffusion between domains (Jalowiecki *et al* 1996). In conclusion, both regulation of processing parameters and better selection of doping elements can result in more thermodynamically stable PDCs (Colombo *et al* 2010).

3.2. Electrical conductivity

The semiconducting or insulating behavior of a PDC is strongly influenced by its pyrolysis temperature (Cordelair and Greil 2000). Electrical conductivity normally rises with the increase of pyrolysis temperature in accordance with increased percentage of carbon phase (Cordelair and Greil 2000). DC-conductivities published recently for PDCs pyrolyzed at relatively lower temperatures (between 600 °C–800 °C) demonstrates a change within the limit of 10^{-10}–10^{-8} $(\Omega\ \mathrm{cm})^{-1}$ (Cordelair and Greil 2000, Haluschka *et al* 2000, Kroll 2003). It has been observed that semi-conductivities (10^{-4}–10^{2} $(\Omega\ \mathrm{cm})^{-1}$) or even higher conductivities (~10^{4} $(\Omega\ \mathrm{cm})^{-1}$) are observed for PDCs sintered at about 1000 °C–1400 °C, due to the establishment of percolation networks of carbon (Cordelair and Greil 2000). It is possible for PDCs pyrolyzed at temperatures higher than 1400 °C to obtain even higher electrical conductivities, due to the formation of nanocrystalline phases (Haluschka *et al* 2000).

3.3. Mechanical properties

In tensile testing, most PDC fibers demonstrate approximately 1–3 GPa in tensile strength (Colombo *et al* 2010). An elastic modulus of 170–400 GPa is obtained, which is slightly higher than that of bulk PDCs at 95–155 GPa. Reduction in oxygen contamination has also been shown to lead to elevated high-temperature stability and modulus (Shah and Raj 2002). Still, the elastic modulus of conventional ceramics is significantly higher than both fiber and bulk, indicating the lower density of PDCs (Colombo *et al* 2010). The elastic behavior of PDCs is a function of atomic structure and covalent bonding. For example, in the SiOC system, the free-carbon network contributes towards stiffness while oxygen from the silica tetrahedral maintains flexibility (Kroll 2003, Kumar and Kim 2010). The density of bulk SiOC or SiCN varies from 1.8 g cm^{-3}–2.3 g cm^{-3} with increase of sintering temperature because of more hydrogen being extracted from C–H bonding, which also leads to a less amorphous structure. This also has beneficial effects on elastic modulus and mechanical strength (Colombo *et al* 2010).

3.4. Processability

Conventional fabrication methods such as extrusion, injection molding and hot/cold pressing, etc, can be used in developing PDCs. Moreover, processing complicated structures such as 1D fibers, 2D films and 3D shell/core nanocomposites is possible because of the ease of their polymer-to-ceramic processing route (Yajima *et al* 1976, Bill and Heimann 1996, Baldus *et al* 1999, Cross *et al* 2006, Singh *et al* 2009, Bedekar *et al* 2010, Lehman *et al* 2010, Bhandavat *et al* 2012a, Bhandavat and Singh 2012b). Extraordinarily, a direct processing polymer-to-ceramic approach enables achieving uniformly distributed microstructure (Kumar and Kim 2010). The porosity of the PDCs is manipulated by either changing processing parameters—such as by introducing additives, altering pyrolysis temperature and atmosphere, or applying different processing strategies—such as templating, etching, blowing, decomposition, aerogels and spinning (Vakifahmetoglu *et al* 2016). It has been reported by Vakifahmetoglu *et al* that porous PDCs can have specific surface area up to 3000 m^2 g^{-1} with volumetric porosity of 15%–96% and pore size of approximately 1–1.5 mm (Vakifahmetoglu *et al* 2016). Erb and Lu have demonstrated the possibility of obtaining PDCs with varying porosity and ceramic content based on the presence of vinyl bonds in the precursor polymers (Erb and Lu 2018).

4. Experimental results on PDCs in electrochemical energy storage systems

The application of PDCs as electrode materials in different electrochemical energy storage systems (LIBs, SIBs, supercapacitors) will be discussed in detail in the subsequent sections. The discussion will not only focus on the performance parameters, but will look at how other important criteria—processing parameters, molecular structure and composition of the precursors, etc—affect the performance. It is to be noted that PDCs have primarily found application as negative electrode materials (anodes) in energy storage systems, and the following sections will therefore look at their performance accordingly.

4.1. PDCs as negative electrodes in LIBs

A significant amount of scientific research on silicon-based nanomaterials has been carried out, especially as negative electrodes for electrochemical energy storage devices, owing to silicon's favorable properties (Bourderau *et al* 1999, Chan *et al* 2008). Specifically, Si's ability to form a binary system with Li leads to a high theoretical energy density up to 4200 mAh g^{-1}, which is an order of magnitude greater than commercial graphite anodes in Li-ion batteries, as well as less potential in discharge (Dahn *et al* 1995, Winter *et al* 1998, Saint *et al* 2007, Zhang 2011). However, the primary drawback of Si is that the material may experience volumetric changes of up to 400% on lithiation and delithiation, which results in electrode pulverization and considerable capacity fading (Obrovac and Christensen 2004).

One way of overcoming this problem has been to use silicon-based PDCs and not the silicon in its pure elemental form. Silicon based porous PDC anode materials have been investigated with favorable outcomes to this end. Literature/the current state-of-the-art demonstrates that amorphous PDCs can reversibly store lithium within the voltage boundary between 0.0–3.0 V while providing promising electrochemical capacity up to 900 mAh g^{-1}, as well as coulombic efficiency (CE) surpassing 99%. Other advantages of PDCs lie in their open amorphous but thermodynamically stable structure and processability. However, their characteristic first cycle loss (a composition dependent 27%–50% loss) and hysteresis at a potential window of 0.8–1.2 V are issues that still need to be overcome. Modification of the pre-ceramic polymer's structure to achieve elevated surface area (porosity) and the addition of electrochemically favorable conducting nanofillers are some of the solutions that have been proposed.

For application as electrode material, plenty of effort have been devoted mainly to the following two systems: SiOC, derived from polysiloxane, and SiCN, derived from polysilazane. While some drawbacks of these systems have been identified, researchers have focused on PDC based composites as well. The following sections will discuss the application and performance of these three types of PDC system as negative electrode materials in LIB systems.

4.1.1. The Si–C–O ternary phase. The Si–C–O system is characterized by the presence of Si, C and O atoms bonded together to form an amorphous structure (Mazo *et al* 2016). Free carbon, if present, prevents the crystallization of the silica phase. The network of the bonds and the free C content also control the oxidation resistance of the ceramic (Mazo *et al* 2016). The phase diagram of the Si–C–O ternary system is represented schematically in figure 4. As can be observed from the figure, the light blue shaded zone is where the maximum capacity (solid red squares) region occurs, as SiO and SiC co-exist here with free C.

Bulk SiOC systems were first studied by Wilson *et al* when they conducted initial investigations on SiOC PDCs derived from polysiloxanes about their reversible lithium ion insertion properties (Wilson *et al* 1994). They have successfully demonstrated capacities up to 600 mAh g^{-1} within 1 V. Xing *et al* carried out a parametric study of 64 different SiOC samples with different chemical concentrations (Xing *et al* 1997). They have demonstrated SiOC with 14% Si and 80% C to be the best commercially recommended material—over 25% Si, 45% C and 30% O combination—with higher reversible capacity and voltage hysteresis. Also, SiOC PDCs have performed better than crystalline SiO+C with equal Si, O and C concentrations (Xing *et al* 1997). Kaspar *et al* carried out a study on polyorganosiloxane derived SiOC processed at temperatures ranging from 900 °C to 2000 °C (Kaspar *et al* 2013). They have noticed a decrease in reversible capacity with increasing processing temperature (from 666 mAh g^{-1} to 73 mAh g^{-1} at current rate of 37 mA g^{-1}). Both XRD and FTIR results indicated the amorphous structure of samples pyrolyzed below 1200 °C, while additional SiC domains formed continuously at higher temperature (Kaspar *et al* 2016a). By mixing hydrogen with argon, Pradeep *et al* studied the impact of pyrolysis atmosphere on SiOC composition and its electrochemical performance (Pradeep *et al* 2014b). They observed that 5% of H_2 caused significant reduction in C concentration 55.15 wt.% to 46.37 wt.%; however, it elevated first cycle capacity (from 568 to 704 mAh g^{-1}) and efficiency (from 63 to 67%) (Pradeep *et al* 2014b). Additionally, Ahn *et al* focused their investigation on the significant hysteresis in SiOC as anode material in Li-ion batteries. They used a coulometric titration technique for this purpose and have demonstrated hysteresis at a polarization potential of 250–500 mV (Ahn and Raj 2010). This was attributed to the interface between anode and electrolyte, where the potential grows with increasing cycling (Ahn and Raj 2010). From the measurement, the hysteresis was found to be a product of both thermodynamic limitations and kinetics of Li-ion diffusion between the different electrochemical potentials of Li-ions at SiOC–electrolyte and lithium–electrolyte surfaces (Ahn and Raj 2010). Further measurement by Ahn *et al* was extended to the pre-ceramic polymer precursor chemistry with variable composition of N and O in a SiOCN quaternary system (Ahn and Raj 2011). Results have shown far better performance in O-rich while very poor capacity for Ni-rich samples, where capacity changes rapidly with dominant element near the ratio of N/O = 1. It has also been demonstrated that the SiOC structure is more stable than SiCN under the same conditions (Ahn and Raj 2011). Stronger covalent bonding in tetrahedral Si–N resulted in low efficiency in Li-ion binding and electron density localization than bonds in Si–O nanostructure (Ahn and Raj 2011). Approximately 100% capacity is recovered after 60 cycles for samples pyrolyzed at 800 °C and 1000 °C,

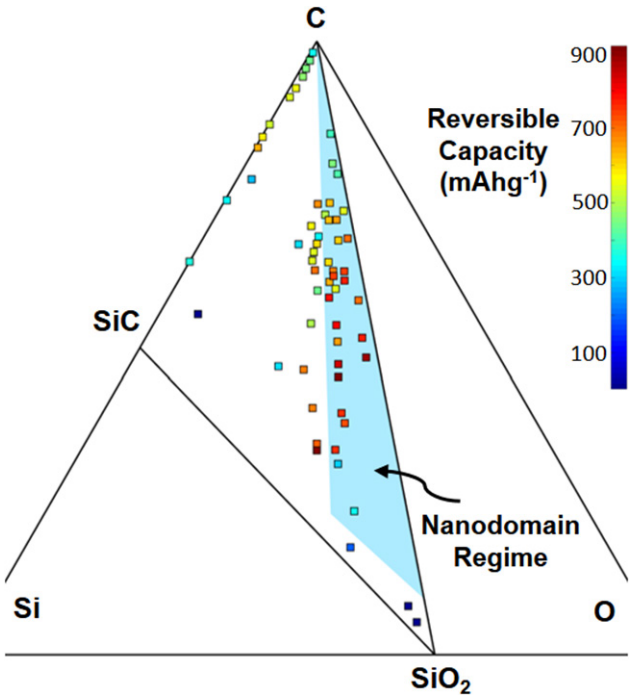

Figure 4. The Si–O–C phase diagram. The phase diagram of the Si–O–C ternary system, the shaded area towards the center of the 'pyramid' represents the tetrahedral ceramic phase consisting of mixed bonds and consisting of nanodomains. Reproduced with permission from (Xing *et al* 1997).

compared to the significant drop for samples pyrolyzed at 1200 °C and 1400 °C (Ahn and Raj 2011). Fukui *et al* have studied the process of fabricating porous PDCs by increasing active surface area, which ultimately enhanced reversible capacity and cyclic performance (Fukui *et al* 2009, 2011c). In their study, blending of polystyrene and branched polysilanes was used to produce porous specimens having pore sizes of ~2 nm and surface areas of ~14 m^2 g^{-1}. The best reported result was a reversible capacity of 565 mAh g^{-1} and 73% efficiency for $SiO_{0.4}C_{0.8}$ ceramics (Fukui *et al* 2009, 2011c). Li ions have been demonstrated to be stored here in small quantities and in an ionized form. In a later work, they have also applied the microelectrode technique to SiOC single particles with diameter of 13 μm at 5 nA (4 C-rate) and have obtained 98% of coulombic efficiency after first cycle, which shows strong agreement with porous electrodes (Fukui *et al* 2011a).

Thin-film SiOC anode materials have been studied on account of their flexible processing techniques (Shen and Raj 2011). Experiments with SiOC films of 0.5–5 μm thickness demonstrate performances comparable to bulk SiOC ceramics (Shen and Raj 2011). SiOC thin films have the added advantage of being completely free from additives, which helps to reduce battery weight by significant amounts. The SiOC films showed reduced first cycle loss down to 27%, maintained capacity at about 1100 mAh g^{-1} and approximately 99% of cycle efficiency (Shen and Raj 2011). The authors have observed that the thickness of the film influences the diffusivity of the Li ions (Shen and Raj 2011).

Etching effect of KOH on SiOC anodes was specifically studied by Xia *et al* with various weight ratios (3:1, 5:1, 7:1) of KOH to vinylteriethoxysilane derived SiOC ceramics (Xia *et al* 2017). Etched SiOC sample (with 5:1 weight ratio of KOH:pre-ceramic polymer) exhibited the highest specific surface area (249.2 m^2 g^{-1}) and reversible capacity (607 mAh g^{-1}) after 50 cycles, thereby revealing enhanced electrochemical properties with appropriate etching ratios. However, the authors have noted that high etchant concentrations may negatively affect the electrochemical performance due to destruction of the free carbon phase (Xia *et al* 2017).

Effect of electrolyte on the cyclability of the SiOC ceramic anode based LIBs have been carried out by Seko *et al* (2017). As electrolytes, triglyme: G3 (Li(G3)TFSI) and tetraglyme: G4 (Li(G4)TFSI) have been used with various additives such as fluoroethylene carbonate (FEC) and vinylene carbonate (VC). The highest initial capacity (1418 mAh g^{-1}) has been reported using Li(G4)TFSI without additives; however, lower capacity (1322 mAh g^{-1}) coupled with better cyclability (101% after 100 cycles) was obtained using Li(G4)TFSI with FEC (Seko *et al* 2017). Therefore, according to Seko, 'activation' without additives is recommended to improve the initial capacity. Retention of capacity is then achievable via additives after the first cycle (Seko *et al* 2017).

Li ion insertion mechanisms have been studied by Liu *et al*, who carried out a series of characterization techniques (including ^{29}Si MAS NMR, Si XPS and CV) for this purpose (Liu *et al* 2011). The NMR, XPS and CV were performed at three different stages (original, full lithiation and complete delithiation) of SiOC samples, and SiO_2 and Si for comparison. The authors have noted four resonances to exist in the SiOC samples—namely, SiO_4, SiO_3C, SiO_2C_2 and $SiOC_3$—in which SiO_3C, SiO_2C_2 are electrochemically active to Li-ions dominating reversible capacity, while $SiOC_3$ is irreversibly converted into SiC_4 after the first cycle (Liu *et al* 2011). A new insight has been proposed by Pradeep *et al* about the Li storage mechanism (Pradeep *et al* 2014a). The comparison between two sets of SiOC pyrolyzed at 1000 °C and 1300 °C revealed a composite-like behavior of $SiC_xO2_{(1-x)}$ glass phase and free carbon phase (Pradeep *et al* 2014a). Whereas $SiC_xO_{2(1-x)}$ provides a first insertion capacity as high as 1300 mAh g^{-1}, the cyclability and reversibility are dominated by free C (Pradeep *et al* 2014a). Fukui *et al* have analyzed the Li storage mechanism and first cycle loss in SiOC species (Fukui *et al* 2014). They have demonstrated that the nature of Li species stored is mostly ionic from the ^{7}Li MAS NMR spectra (figure 5(a)), and that only 30% of Li is reversible when cycled between 0.4–3.0 V (Fukui *et al* 2014). This ionic nature is seen in greater detail in figure 5(b), which shows a SiOC resonance peak at almost 0 ppm (Fukui *et al* 2014). More recently, Zhao *et al* investigated electro-chemo-mechanical effects of lithiation in carbon-rich SiOC using the first-principles approach (Sun and Zhao 2017). Their research suggests that Li insertion in SiOC is a two-step process: the Li is first absorbed at the nanovoids; this is followed by Li accommodation in SiOC tetrahedral units, free C atoms, and topological defects in and around the carbon network. The SiOC expanded by approx. 22% in volumetric strain at its full lithiation capacity and the surrounding carbon network improved the structural stability of the SiOC lattice (Sun and Zhao 2017). The schematic of this process is depicted in figures 5(c) and (d).

4.1.2. The Si–C–N ternary system. The Si–C–N system is obtained from polysilazanes and consists of C and N rich nanodomains if the pyrolysis is at low temperature; however, high temperature pyrolysis results in the formation of Si_3N_4 and SiC rich regions instead (Bernardo *et al* 2014). The phase diagram schematic is shown in figure 6.

Bulk SiCN systems were studied by Liebau-Kunzmann *et al* who were among the earliest to suggest the possibility of applying SiCN PDC based electrodes in lithium ion batteries (Liebau-Kunzmann *et al* 2006). In their study, Li-containing SiCN PDCs were synthesized at 1100 °C, and subsequent characterization showed preferential formation of Li–N bonds during lithiation, indicating potential for anode application (Liebau-Kunzmann *et al* 2006).

Temperature dependent electrochemical properties of SiCN PDCs for anode application have been studied by Su *et al* (2009). It has been shown that samples synthesized at 1000 °C–1300 °C showed the most favorable first reversible capacity up to 754.9 mAh g^{-1} (Su *et al* 2009). The authors have also demonstrated that fabrication temperatures any higher or lower provide significantly lower capacities, just in excess of 100 mAh g^{-1}. They have attributed this to remnant organics under 800 °C and crystalline SiC formed above 1400 °C, both of which blocked the path for efficient Li ion intercalation and storage (Su *et al* 2009). In addition, study on lithiation into carbon-rich SiCN derived by poly-diphenyl-silyl-carbodiimide

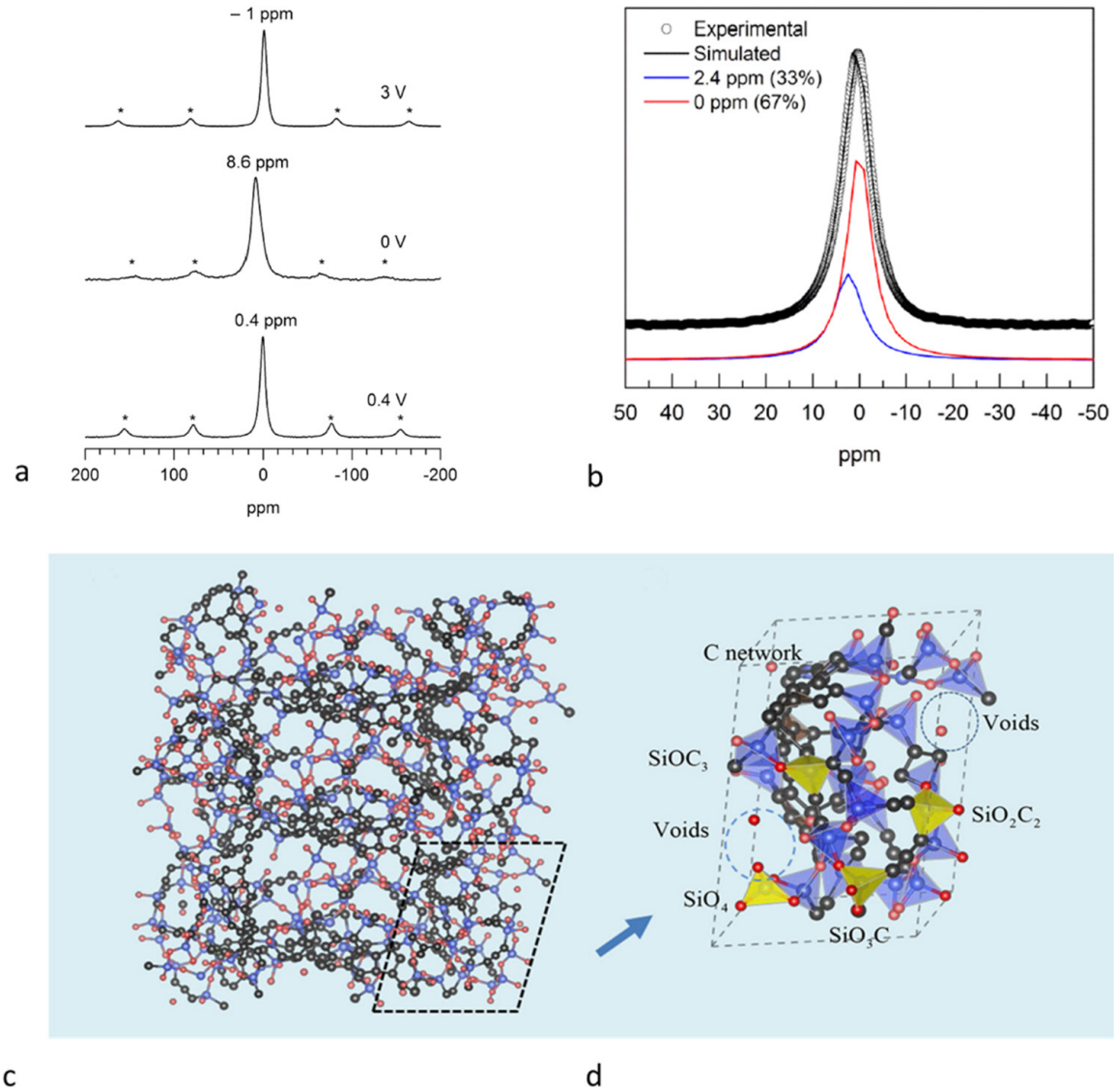

Figure 5. Understanding lithiation in SiOC. (a) Experimental ^{7}Li MAS NMR spectra of SiOC cycled between 0.005–3 V, lithiation up to 0 V and partial lithiation to 0.4 V, from top to bottom respectively (Fukui *et al* 2014). (b) Experimental and simulation comparison of the ^{7}Li MAS NMR spectra of the SiOC sample which has undergone partial lithiation up to 0.4 V (Fukui *et al* 2014). Atomistic modeling: atomistic model of silicon oxycarbide. (c) Supercell with an applied periodic boundary condition (Sun and Zhao 2017). (d) Unit cell-vertex-sharing Si tetrahedra, nanovoids (blue dotted circle), and segregated C phase (gray atoms) are clearly marked (Sun and Zhao 2017). (a), (b) Reprinted with permission from (Fukui *et al* 2014). Copyright 2014 American Chemical Society. (c), (d) Reprinted with permission from (Sun and Zhao 2017). Copyright 2017 American Chemical Society.

has been performed by Kaspar *et al* specifically at the temperatures of 1100 °C, 1300 °C and 1700 °C (Graczyk-Zajac *et al* 2010, Kaspar *et al* 2010). Among these additive free samples, the one synthesized at 1300 °C performed the best, demonstrating 383 mAh g^{-1} reversible capacity and 69% coulombic efficiency and confirming that the free carbon phase provides enhanced electrochemical performance by making more active sites available (Graczyk-Zajac *et al* 2010, Kaspar *et al* 2010).

Molecular structure of pre-ceramic polymer's effects on electrochemical properties have been studied by Reinold *et al* (2013). Different classes of pre-ceramic polymer—namely, polysilazane and poly-silyl-carbodiimide—were processed under the same conditions (1100 °C, Ar) revealing higher reversible capacities of 724 mAh g^{-1} and 612 mAh g^{-1} respectively (Reinold *et al* 2013). Similarly, coulombic efficiency of 89% to 61% (after 134 cycles), correspondingly for polysilazane derived ceramics and poly-silyl-carbodiimide derived ceramics were obtained, showing the consistently superior performance of the polysilazane pre-ceramic polymer (Reinold *et al* 2013).

Variation of pyrolysis environment on SiCN's performance as an electrode has been studied by Liu *et al* (2013). A variation in the pyrolysis atmosphere from Ar to H_2 demonstrated higher constituent C content and a higher reversible capacity (Liu *et al* 2013). Additional free carbon source from divinylbenzene (DVB) has been shown to further increase the carbon content (from 9.9 wt.% to 49.3 wt.%) and specific capacity (from 136 mAh g^{-1} to 574 mAh g^{-1}), while providing slightly increased hysteresis under 1 V (Liu *et al* 2013). To further improve the electrochemical performance, heat treatment has been applied to poly-

silyl-ethylenediamine derived SiCN ($SiN_{0.31}C_{0.97}H_{0.31}O_{0.05}$) under 1000 °C in argon by Feng, resulting in the formation of nano-voids on the surface as well as enriched free carbon phase (Feng 2010). The analysis indicated improved reversible capacity (above 300 mAh g^{-1}) even at high current (80 and 160 mA g^{-1}) for treated SiCN ($SiN_{0.18}C_{0.41}H_{0.91}O_{0.10}$) (Feng 2010). The enhancement was generally due to decrease of N content and increased O contamination during the heat-treatment (Ahn and Raj 2010). In general, the lithium intersection capacity of SiCN PDCs is strongly determined by the formation of amorphous graphene phase and nano-voids in the structure.

Capacity fading mechanism of SiCN was recently studied by Feng *et al* employing five different poly-silyl-carbodiimides as pre-ceramic precursor (Feng *et al* 2017). They concluded that stable SEI layers formed on the surfaces of anodes prevent fracture of active materials during cycling (Feng *et al* 2017). Besides, more carbon phase improves electrochemical conductivity and enhances the reactive sites in SiCN anodes. Therefore, the di-n-octyldichlorosilane (DODCS) synthesized poly-silyl-carbodiimide sample, containing the highest carbon composition, resulted in the highest reversible capacity of 826.7 mAh g^{-1} after 100 cycles with coulombic efficiency above 97% (Feng *et al* 2017).

A comparison of the electrochemical performance of SiCN and SiOC is provided in figure 7 along with SiOC's performance as a function of pyrolysis temperature.

4.1.3. PDC-carbon nanomaterial composites. Simple PDC based anodes in their various forms—bulk as well as thin film, crystalline and amorphous—pose several hurdles such as first cycle loss, voltage hysteresis and capacity decay, and improvements therefore still need to be made.

Incorporating carbon nanomaterials (such as CNTs and graphene) into PDCs has recently been proposed as a solution (Kim *et al* 2006, Landi *et al* 2009, Liu *et al* 2012b). Superior properties of these nanomaterials include high aspect ratio, which leads to better flexibility, extremely high electron mobility, shorter diffusion length, light weight and stronger mechanical behavior.

As an illustration, as shown in figure 8, volumetric changes after charge and discharge often causes separation of active particles. The specific capacity ultimately degrades because of this progressive cycling. Introducing CNTs into the active material corrects electronic or ionic conductivity loss from volumetric changes, thus decreasing capacity decay.

Konno *et al* studied pyrolysis of polysiloxane compounds and exfoliated graphite at 1000 °C–1300 °C, producing a SiOC–graphite composite with an average composition of $SiOC_{1.1}$ (Konno *et al* 2005). Above 600 mAh g^{-1} of reversible capacity with first cycle loss of 30% was reported; moreover, the capacity was stable under high current density (100 mA g^{-1}) (Konno *et al* 2005). Later, Ji *et al*, in their work using self-assembly of graphite oxides, successfully synthesized SiOC–graphite nanosheet composite anode material that exhibited a reversible capacity of 364 mAh g^{-1}, containing 25 wt.% of graphite (Ji *et al* 2009). Kolb *et al* followed a different approach, using commercially available graphite and

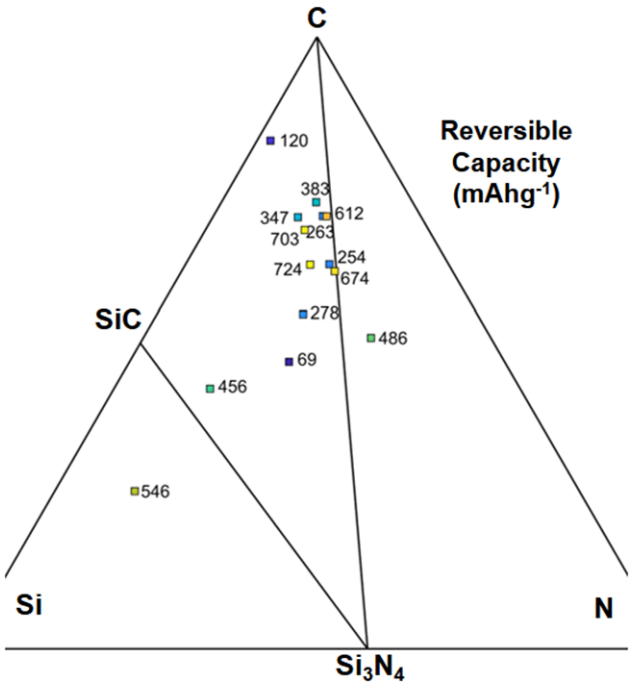

Figure 6. The Si–C–N phase diagram. The phase diagram of the Si–C–N ternary system; once again, the maximum capacity regime occurs towards the center of the pyramid, where the Si_3N_4 and SiC phases coexist (Reinold *et al* 2015).

cross-linked polysilazane (wt. ratio 3:1) pyrolyzed at 1050 °C (Kolb *et al* 2006). The SiCN–graphite sample demonstrated a first discharge capacity of 474 mAh g^{-1}, 1.3 times higher than pure graphite under the same conditions. According to the authors, this enhancement is due to the formation of a stable protective SiCN layer on graphite, which prevents the exfoliation of the graphite phase (Kolb *et al* 2006). Similarly, with weight ratio of 1:1, Graczyk-Zajac *et al* reported that SiCN-graphite composite anodes synthesized at 950 °C, 1100 °C and 1300 °C could recover more than 80% of capacity under 1 V (Graczyk-Zajac *et al* 2011). Among the three samples, the sample prepared at 950 °C provided the highest reversible capacity of 376 mAh g^{-1}, with a 72% first cycle efficiency (Graczyk-Zajac *et al* 2011).

Along similar lines, Ahn *et al* have demonstrated performance of SiOC-graphene composite via mixing liquid phase graphene oxide and polysiloxane precursors which provided a uniform composition when synthesized (Ahn *et al* 2010). Anodes produced by this technique have demonstrated specific capacities beyond 800 mAh g^{-1} even after 500 cycles (Ahn *et al* 2010). Figure 9 shows the comparative mechanism and electrochemical performance of SiCN and SiOC systems coupled with graphene and reduced graphene oxide (rGO) as composites

Apart from graphite and graphene additives, carbon nanotubes (CNTs) as composites with PDCs have also received research focus. Shen *et al* has focused on improving high charge rate properties of SiOC-CNT composites made of single wall carbon-nanotube and SiOC PDC powder (Shen *et al* 2011). A stable capacity of 515 mAh g^{-1} of stable capacity was achieved at a current density of 8500 mA g^{-1} (16.5

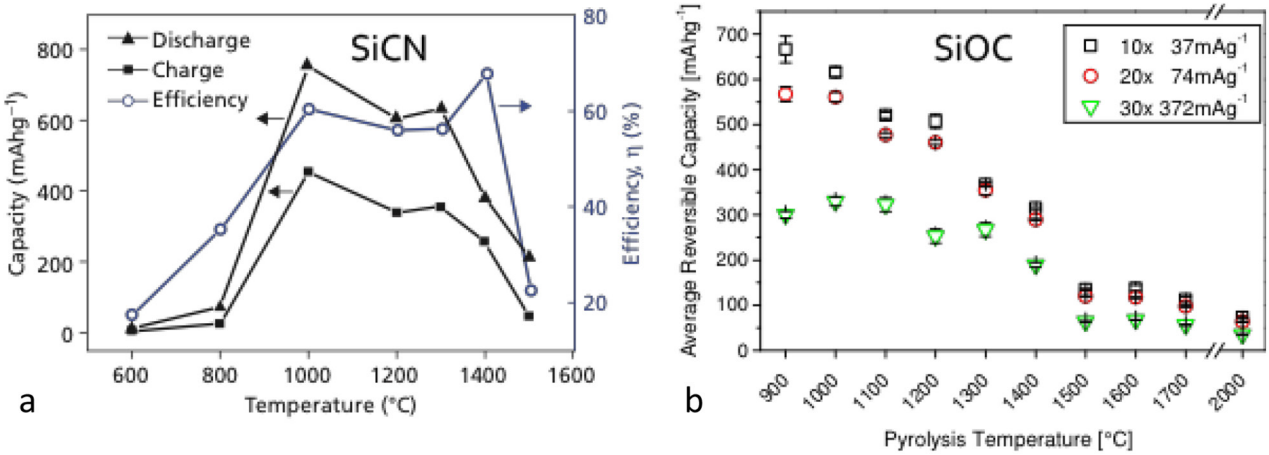

Figure 7. Comparative electrochemical performance of SiOC and SiCN with respect to pyrolysis temperature. (a) Comparison of electrochemical performance (charge & discharge capacities, efficiency) of SiCN specimens pyrolyzed at increasing temperatures. (Su *et al* 2009). John Wiley & Sons. © 2009 The American Ceramic Society. (b) SiOC average reversible capacity in dependence of temperature of pyrolysis. Average values were calculated from ten cycles (Kaspar 2014).

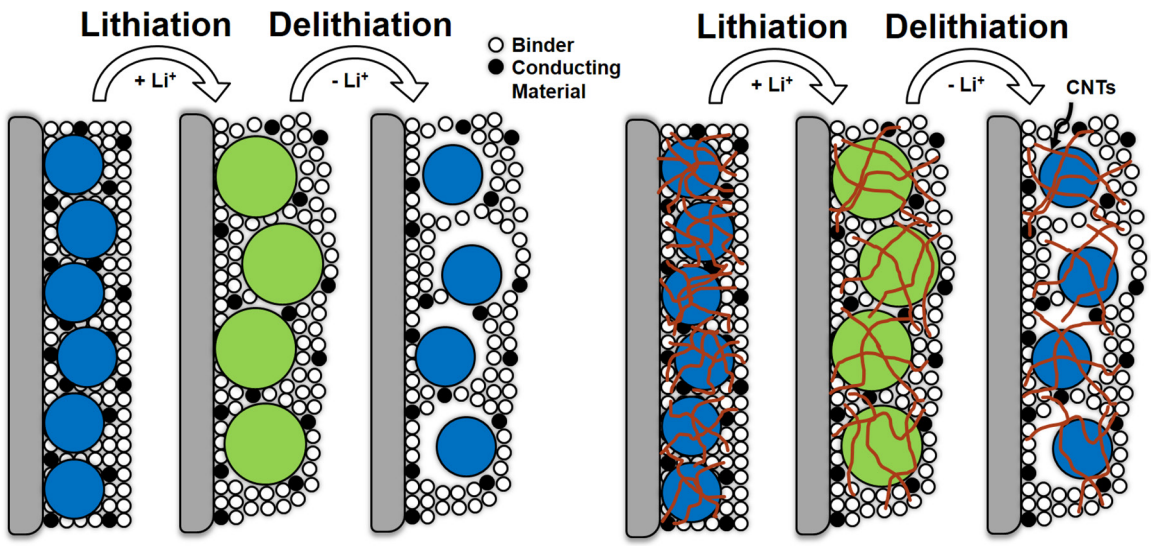

Figure 8. Phenomenological understanding of effect of Li intercalation on PDC-carbon composites. Step-by-step comparison of the effect of lithium intercalation and deintercalation in the silicon particle electrode with and without carbon nanotubes as conducting agents.

C-rate) which was attributed to increased conductivity and superior cyclic stability of CNTs (Shen *et al* 2011).

CNT enhanced high-rate capability of SiCN was also studied by Zhang *et al* via pyrolysis of ultra-sonicated multi-walled CNT and polysilazane mixture under 1000 °C in an Ar environment (Lei *et al* 2015). Selected area electron diffraction (SAED) patterns have shown unaffected amorphous structure of SiCN matrix after CNT incorporation. Specific capacity reached 222.7 mAh g^{-1} under a high current density of 2000 mA g^{-1}, superior to that of graphite anodes (about 70 mAh g^{-1} under 100 mA g^{-1}) (Ahn and Raj 2011).

Structural data and electrochemical performance of doped (B and Al) SiCN-CNT composite systems are provided in figure 10.

In a recent research study on realizing high capacity electrodes, Vrankovic *et al* attempted to embed organic carbon coated porous silicon in polysilazane derived SiOC/C (pyrolyzed at 1100 °C) matrix (Vrankovic *et al* 2017). Silica and sol–gel derived nanoparticles (NPs) were subjected to alumino-thermic and magnesio-thermic reduction accompanied by HCl etching and pyrolysis at 1100 °C. Electrochemical measurement demonstrated greater than reversible specific capacity of 2000 mAh g_{si}^{-1} (400 mAh $g_{composite}^{-1}$) capacity with 99.5% coulombic efficiency after 100 cycles (Vrankovic *et al* 2017). This performance has been attributed to the adjustment of volumetric changes by open Si structure, enhanced electronic and ionic conductivities provided by the carbon phase, and minimized SEI formation due to the SiOC encapsulating effect (Vrankovic *et al* 2017).

Li *et al* have recently proposed a SiOC/C binder-free composite anode material synthesized using an electrospinning technique (Li *et al* 2014). The 1,3,5,7-tetramethyl-1,3,5,7-tetravinylcyclotetrasiloxane (TTCS) pre-ceramic precursor and polyacrylonitrile (PAN) mixture were electrospun to produce fibers and then pyrolyzed at 700 °C in Ar (Li *et al* 2014). A first cycle reversible capacity of 839 mAh g^{-1} and

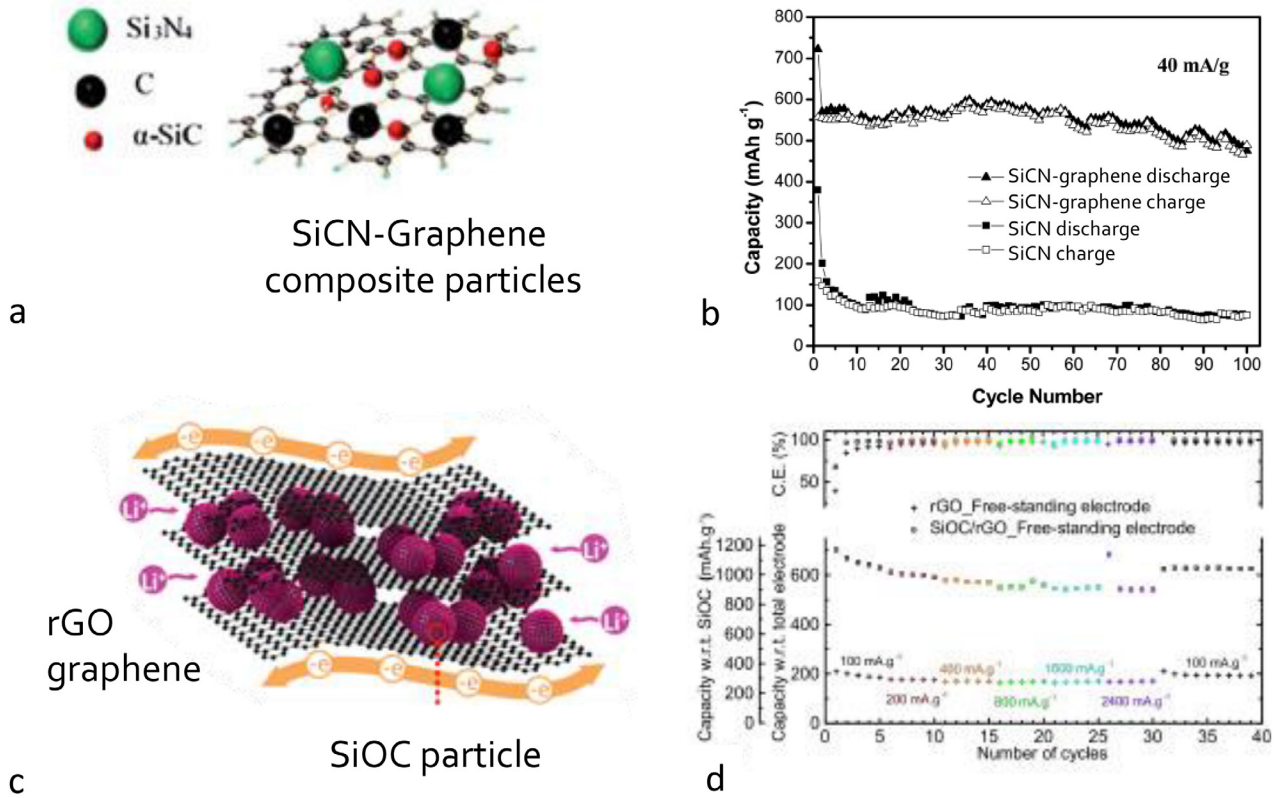

Figure 9. Schematic of PDC-composite structure and performance. (a) Structure of SiCN-graphene composite (Feng *et al* 2014). (b) Cyclability performance of SiCN, SiCN-graphene electrodes (Feng *et al* 2014). (c) Schematic of SiOC-rGO layered composite paper electrode (David *et al* 2016a). (d) Cyclability performance of SiOC/graphene and rGO graphene electrodes (David *et al* 2016a). (a), (b) Reproduced from (Feng *et al* 2014) with permission of The Royal Society of Chemistry. (c), (d) (David *et al* 2016a) Copyright © 2016 Springer Nature. With permission of Springer.

subsequently 669 mAh g^{-1} after 80 cycles was reported. As the matrix, carbon phase adjusted volumetric changes of SiOC and provided extra free carbon to the system which enhanced cyclability (Li *et al* 2014). Boron modified polysilazane derived Si(B)CN ceramic coated multi-walled CNT composite material provided electrochemical capacity of 412 mAh g^{-1} (at 30 cycles) (Bhandavat *et al* 2012a). Si(B)CN CNT composite has been synthesized by use of microwave assisted pyrolysis and conventional heating. Microwave heating greatly reduces the processing time with a ceramic yield of approximately 50%. Si(B)CN-CNT composite prepared via microwave assisted pyrolysis has a higher Si/N atomic ratio compared to conventionally produced Si(B)CN (4.75 versus 0.77). The higher Si/N ratio is believed to improve the electrochemical cycling performance of the composite (Bhandavat *et al* 2012a). In addition, the core–shell structure of the ceramic improved stability and electrical and ionic conductivity when compared to traditional powdered SiCN PDC anodes (Bhandavat *et al* 2012a).

4.2. Performance of PDCs as negative electrodes in SIBs

SIBs tend to overcome some of the important deficiencies of LIBs—namely, reduced materials and fabrication cost, use of less toxic electrolytes and greater suitability for large scale grid storage. However, due to the limitations imposed on the choice of electrode in SIBs as discussed in section 2, it is necessary that novel materials be tried out for this purpose. PDCs have been studied as anode materials in SIBs as well; to a much lesser extent, however, than LIBs. A few prominent works are listed in the following discussion.

Lee *et al* studied an Sb embedded SiOC as an anode in SIBs (Lee *et al* 2017). A 'one pot pyrolysis' technique was used to fabricate the PDC composite at a temperature of 900 °C (Lee *et al* 2017). A first cycle de-sodiation capacity of 510 mAh g^{-1} was observed; 97% of the capacity was retained after 250 cycles. The composite also delivered 453 mAh g^{-1} at 20 C-rate. The free carbon phase in the SiOC phase was deemed to be responsible for this performance (Lee *et al* 2017). Using silicone oil as a precursor, SIOC anodes for SIBs have been studied by Chandra and Kim (2018). The fabrication involved pyrolysis of the oil in an Ar environment at varying temperatures (700 °C, 800 °C, 900 °C) followed by mechanical milling and pulverization (Chandra and Kim 2018). The sample obtained at a calcination temperature of 900 °C demonstrated the best results, delivering a specific capacity of 160 mAh g^{-1} at a current density of 25 mA g^{-1} after 200 cycles of operation (Chandra and Kim 2018). The stability demonstrated by this sample was also high, losing just 0.09 mAh g^{-1} of specific capacity after 650 cycles of operation. The authors have attributed the performance to well-developed SiOC phase and presence of significant free carbon (Chandra and Kim 2018).

The effect of morphology of a SiOC(N)/hard carbon composite as an anode material has been studied by Kaspar *et al* (2016b). Variation in the composite was introduced by varying

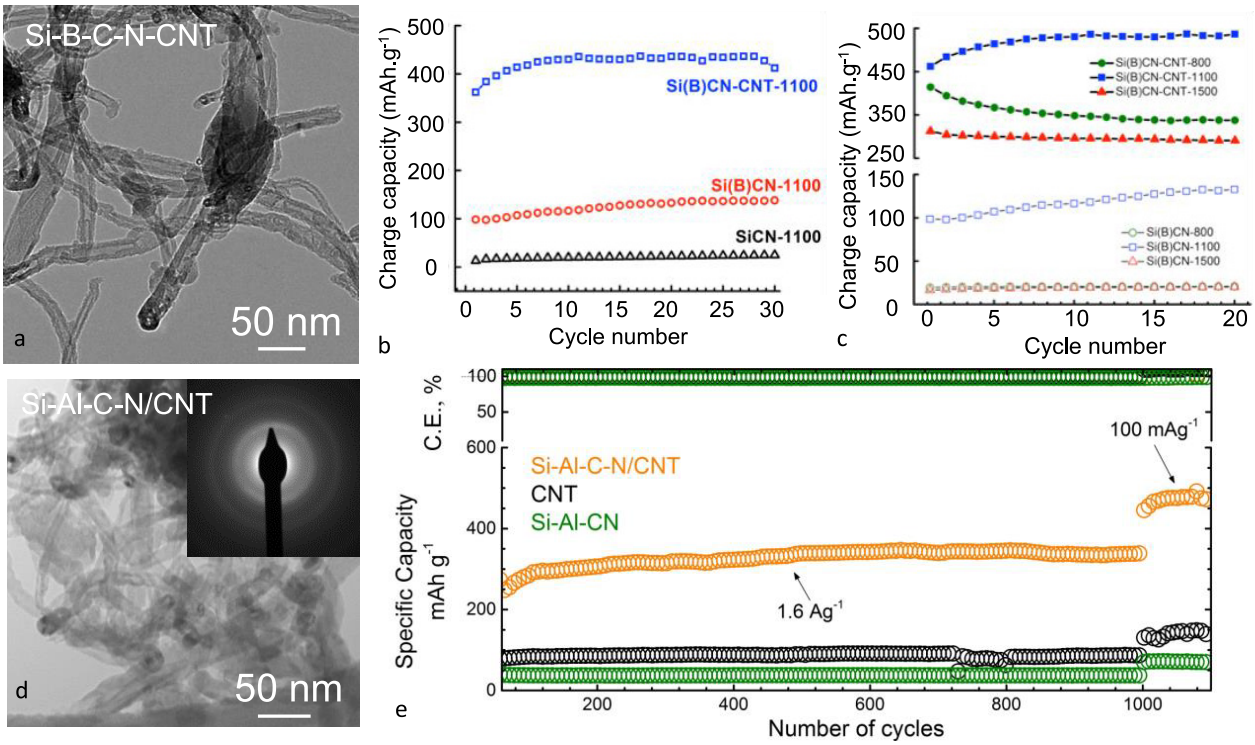

Figure 10. Performance of PDC-CNT composite anode systems. (a) TEM of SiBCN/CNT composite nanotubes. (b) Cyclability performance of SiCN, Si(B)CN and Si(B) CN-CNT composite anodes (Bhandavat and Singh 2012a). (c) Optimum performance (least first cycle loss and highest charge capacity) was observed for specimen synthesized at ~1100 °C (Bhandavat and Singh 2012a). (d) TEM of SiAlCN/CNT composite nanotubes (David *et al* 2014). (e) Long-term cycling performance of SiCN, SiAlCN and SiAlCN/CNT composite electrodes (David *et al* 2014). (b), (c) Reprinted with permission from (Bhandavat and Singh 2012a). Copyright (2012) American Chemical Society. (d), (e) Reprinted with permission from (David *et al* 2014). Copyright 2014 American Chemical Society.

the carbon source (glucose and potato starch), ceramic precursor (RD-684a, HTT1800) and the ratio (1:0, 7.7:1, 7.3:1, etc) (Kaspar *et al* 2016b). Results indicate samples with low oxygen content (<10 wt.%) and mesoporous morphology tend to provide high specific capacities: 262 mAh g^{-1} and 201 mAh g^{-1} respectively (Kaspar *et al* 2016b).

Table 1 summarizes some of the important results when PDCs have been used as anode materials in both LIB and SIBs.

4.3. Performance of PDC electrodes in supercapacitors

Supercapacitors are necessary where the power requirement predominates the energy requirement and it is necessary that charge be stored at or near the surface of the electrode materials. They are usually not constrained by ionic diffusion kinetics experienced in batteries and can run for a large number of cycles (~10^6) at high charge and discharge currents. Therefore, the choice of appropriate electrode materials is necessary for their efficient performance, which necessitates the study of PDC electrodes.

SiOC electrodes in supercapacitors have been studied by several groups. SiOC with low carbon content have been studied by Halim *et al* (2017). Fabrication of the low carbon SiOC was performed by pyrolysis of silicone oil in an inert environment at various temperatures (700 °C–1000 °C in steps of 100 °C) (Halim *et al* 2017). Detailed structural characterization by XRD and TEM have revealed an amorphous nature corresponding to Si–O–C glass structure. Electrochemically, it exhibits a pseudocapacitive behavior providing an energy density as high as 25 W h kg^{-1} with 98.7% capacity retention over 40 000 cycles (Halim *et al* 2017).

Oxygen functionalized high surface area silicon carbide flakes have been studied by Kim and co-workers (Kim *et al* 2016b). The SiC was prepared by a one-step carbonization process followed by an H_2O_2 treatment to introduce surface functionalized oxygen groups (Kim *et al* 2016b). Specific capacitances of 243.3 F g^{-1} have been obtained at scan rates of 5 mV s^{-1} with 85.6% capacitance retention (Kim *et al* 2016b).

SiCN based electrodes have also received attention in supercapacitor applications. Si(B)CN–CNT and SiCN–CNT composites coupled with reduced graphene oxide (rGO) as electrodes in supercapacitors have been studied by David *et al* (2016b). The PDC composites were fabricated by chemical interfacing of pre-ceramic polymer with multi-walled CNTs, which were dispersed in sodium dodecyl benzene sulfonic acid (NaDDBS), in DI water (David *et al* 2016b). A specific capacitance of 269.52 F g^{-1} at a current density of 5 A g^{-1} was reported for the Si(B)CN-CNT-rGO composite electrode (David *et al* 2016b).

SiOC as a precursor for developing nano and mesoporous carbon as electrodes in supercapacitors has also been analyzed (Liqun *et al* 2015, Tolosa *et al* 2016, Yang *et al* 2017). The carbon powders were obtained by mechanical milling of the SiOC precursor followed by subjecting it to chlorine treatment in an evacuated tube at 900 °C followed by NH_3 treatment to

Table 1. An exhaustive list of the various types of PDC system, their fabrication techniques and electrochemical performance as anode materials in LIB and SIB systems.

Specimen (current density)	Synthesis temperature (°C)	First reversible capacity (mAh g^{-1})	First cycle loss (%)	Reversible capacity (mAh g^{-1}) (after *N* cycles)	Reference
SiOC (polysiloxane derived)					
$SiC_{1.83}O_{1.23}$		920	25		Xing *et al* (1997)
SiOC (100 mA g^{-1})	800	906	33	700(60)	Ahn and Raj (2011)
SiOC (100 mA g^{-1})	1000	957	23	650(60)	Ahn and Raj (2011)
$SiC_{0.70}O_{0.01}N_{0.61}$		38	60		Ahn and Raj (2011)
SiOC (37 mA g^{-1})	1100	532	38	521(10)	Kaspar *et al* (2012)
SiOC (18 mA g^{-1})	800	700	6		Graczyk-Zajac *et al* (2012)
SiOC (18.6 mA g^{-1})	1100	719	42		Liu *et al* (2012a)
SiOC, H_2 (50 mA g^{-1})	800	965	42	660(40)	Liu *et al* (2012a)
SiOC thin film (100 mA g^{-1})		1100	27	975(40)	Shen and Raj (2011)
$SiO_{0.93}C_{3.46}$ (18.6 mA g^{-1})[a]	1200	536	39	496(114)	Liu *et al* (2013)
$SiO_{0.95}C_{3.71}$ (18.6 mA g^{-1})[a]	1200	478	44	198(114)	Liu *et al* (2013)
$SiO_{1.00}C_{4.05}$ (18.6 mA g^{-1})[a]	1200	603	38	564(114)	Liu *et al* (2013)
$SiO_{1.03}C_{4.34}$ (18.6 mA g^{-1})[a]	1200	344	45	378(114)	Liu *et al* (2013)
$SiO_{0.90}C_{4.40}$ (18.6 mA g^{-1})	1000	568	37		Pradeep *et al* (2014b)
$SiO_{0.97}C_{3.30}$, 5% H_2 (18.6 mA g^{-1})	1000	704	33		Pradeep *et al* (2014b)
SiOC areogel (360 mA g^{-1})[a]	900	763	49	570(50)	Abass *et al* (2017)
SiOC areogel, H_2 (360 mA g^{-1})[a]	900	919	50	604(50)	Abass *et al* (2017)
$SiO_{1.18}C_{5.52}$ (37 mA g^{-1})[a]	1100	504	36	502(10)	Kaspar *et al* (2016a)
$SiO_{0.95}C_{3.72}$ (37 mA g^{-1})	1100	536	39	524(10)	Kaspar *et al* (2016a)
$SiO_{1.01}C_{2.93}$ (37 mA g^{-1})	1100	434	39	457(10)	Kaspar *et al* (2016a)
$SiO_{0.93}C_{2.26}$ (37 mA g^{-1})	1100	501	38	492(10)	Kaspar *et al* (2016a)
$SiO_{0.87}C_{1.62}$ (37 mA g^{-1})	1100	683	42	555(10)	Kaspar *et al* (2016a)
$SiO_{1.00}C_{1.05}$ (37 mA g^{-1})	1100	706	35	490(10)	Kaspar *et al* (2016a)
$SiO_{1.28}C_{3.67}$ (37 mA g^{-1})	900	738	42	666(60)	Kaspar *et al* (2013)
$SiO_{0.73}C_{3.49}$ (37 mA g^{-1})	1400	313	51	315(60)	Kaspar *et al* (2013)
$SiC_{3.05}$ (37 mA g^{-1})	2000	75	54	73(60)	Kaspar *et al* (2013)
SiOC (25 mA g^{-1})[b]	900	576	33	160(200)	Chandra and Kim (2018)
SiOC (polysilane/polysilycarbodiimide derived)					
SiOC (37.2 mA g^{-1})	1000	608	31	571(50)	Fukui *et al* (2009)
SiOC (37.2 mA g^{-1})	1000	580	32	540(40)	Fukui *et al* (2011c)
SiOC (37.2 mA g^{-1})		573	30		Fukui *et al* (2010)
SiOC:polystyrene (37.2 mA g^{-1})		608	30	577(40)	Fukui *et al* (2011b)
SiOC (polysilsesquioxane derived)					
$SiO_{1.40}C_{0.70}$ (37 mA g^{-1})	1100	501	60	291(10)	Kaspar *et al* (2016a)
SiCN (polysilazane derived)					
SiCN (40 mA g^{-1})	1000	456	40	171(30)	Su *et al* (2009)
SiCN (18 mA g^{-1})	1100	254	53		Kaspar *et al* (2010)
SiCN (18 mA g^{-1})	1300	383	31		Kaspar *et al* (2010)
SiCN (18 mA g^{-1})	1700	120	67		Kaspar *et al* (2010)
SiCN (18 mA g^{-1})	1100	263	57	175(10)	Graczyk-Zajac *et al* (2010)
SiCN, heat treated (40 mA g^{-1})		546	34	371(30)	Feng (2010)
$SiO_{0.06}C_{1.54}N_{0.74}$ (18.6 mA g^{-1})[a]	1200	69	49	88(114)	Liu *et al* (2013)
$SiO_{0.04}C_{2.22}N_{0.84}$ (18.6 mA g^{-1})[a]	1200	278	42	314(114)	Liu *et al* (2013)
$SiO_{0.10}C_{4.04}N_{0.69}$ (18.6 mA g^{-1})[a]	1200	347	40	402(114)	Liu *et al* (2013)
SiCN (74.4 mA g^{-1})	900	447	47	534(100)	Storch *et al* (2018)
SiCN (74.4 mA g^{-1})	1100	282	59	284(100)	Storch *et al* (2018)
SiCN (74.4 mA g^{-1})	1400	240	69	175(100)	Storch *et al* (2018)

(*Continued*)

Table 1. (*Continued*)

Specimen (current density)	Synthesis temperature (°C)	First reversible capacity (mAh g^{-1})	First cycle loss (%)	Reversible capacity (mAh g^{-1}) (after *N* cycles)	Reference
SiCN (polyphenylvinylsilylcarbodiimide derived)					
SiCN (74.4 mA g^{-1})	800	674	44	458(134)	Reinold *et al* (2015)
SiCN (74.4 mA g^{-1})	1300	282	44	308(134)	Reinold *et al* (2015)
$SiC_{5.3}O_{0.2}N_{1.2}$ (18 mA g^{-1})	1100	612	41	584(20)	Reinold *et al* (2013)
SiCN (polyphenylvinylsilazane derived)					
$SiC_{3.9}O_{0.1}N_{0.8}$ (18 mA g^{-1})	1100	703	35	699(20)	Reinold *et al* (2013)
SiCN (polyphenylsilsesquicarbodiimide derived)					
$SiC_{3.0}O_{0.2}N_{1.9}$ (18 mA g^{-1})	1100	486	48	474(20)	Reinold *et al* (2013)
SiCN (polyphenylsilsesquiazane derived)					
$SiC_{3.2}O_{0.1}N_{0.9}$ (18 mA g^{-1})	1100	724	40	715(20)	Reinold *et al* (2013)
PDC composites					
SiOC:GNS (7:3) (40 mA g^{-1})		357	68		Kolb *et al* (2006)
SiCN:graphite (1:3) (0.06 mA g^{-1})		474	35	440(50)	Konno *et al* (2005)
SiCN:G (18 mA g^{-1})	1300	312	24		Graczyk-Zajac *et al* (2011)
SiOC:GO (100 mA g^{-1})		440	37	400(75)	Ahn *et al* (2010)
SiOC:CNT (100 mA g^{-1})		948	35	846(40)	Shen *et al* (2011)
Si(B)CN:CNT (100 mA g^{-1})	1100	362	53	412(30)	Bhandavat *et al* (2012a)
SiOC:exfoliated graphite		625	40	650(15)	Ji *et al* (2009)
SiCN:disordered carbon (1:7.3) (36 mA g^{-1})	1000	570	39	434(400)	Wilamowska *et al* (2013)
SiCN:CNT (9:1) (100 mA g^{-1})	1000	313	48	325(30)	Lei *et al* (2015)
SiBCN:graphene (80 mA g^{-1})	1100	456	46	347(30)	Wang *et al* (2017)
SiOC:nano-crytalline Si (4:1) (74 mA g^{-1})	1100	804		314(50)	Kaspar *et al* (2014)
SiOC:nano-amorphous Si (4:1) (74 mA g^{-1})	1100	555			Kaspar *et al* (2014)
SiOC:BNNT (100 mA g^{-1})	1000	410	51		Lee *et al* (2016)
SiOC:C nanofiber (50 mA g^{-1})	700	839	27	669(80)	Li *et al* (2014)
SiOC:HC (37 mA g^{-1})[b]	1000	201	35	141(50)	Kaspar *et al* (2016b)
SiOC:Sb[b]	900	510	32		Lee *et al* (2017)

[a] DVB modified.
[b] SIB systems.

Table 2. Table depicting synthesis temperature and some notable electrochemical performance of PDCs used as electrodes in supercapacitors.

Specimen (current density)	Synthesis temperature (°C)	Capacitance (F g^{-1})	Power density (kW kg^{-1})	Specific surface area (m^2 g^{-1})	Capacity retention (%) (after *N* cycles)	Reference
SiOC (4.5 A g^{-1})	900		156	3.2	97.5 (40 000)	Halim *et al* (2017)
SiOC-DC (1 A g^{-1})[a]	1000	147		2635.6	94.3 (2000)	Liqun *et al* (2015)
SiOC-DC (0.5 A g^{-1})[a]	1200	163		3122	90.3 (10 000)	Yang *et al* (2017)
SiC-SiOC (0.5 A g^{-1})	1250	259.9		341		Kim *et al* (2016a)
SiOC-DC (0.1 A g^{-1})[a]	1200	135		2394	86 (10 000)	Tolosa *et al* (2016)
SiOC-DC (30 A g^{-1})[a]	1000	86	310	2480	95 (10 000)	Meier *et al* (2014)

[a] SiOC derived carbon.

remove residual chlorine. BET analysis and XRD has shown a decrease in particle size with pyrolysis temperatures greater than 1000 °C and crystalline C powders respectively with no presence of β-SIC impurity phases (Liqun *et al* 2015). Specific capacitance of 148 F g^{-1} has been obtained, with capacitance retention of up to 94.3% after 2000 cycles at current densities of 1 A g^{-1}, in aqueous KOH electrolyte (Liqun *et al* 2015). Along similar lines, Tolosa *et al* obtained nanoporous carbon from SiOC via a chlorine gas treatment at high temperatures of 1200 °C followed by purging with ammonia (Tolosa *et al* 2016). Specific capacitance of 135 F g^{-1} has been obtained, with scan rates of 10 mV s^{-1} and a capacity retention of 63% at current densities of 100 A g^{-1} (Tolosa *et al* 2016). Yang *et al* have been able to derive microporous carbon (surface area of 3122 m^2 g^{-1}) from non-porous SiOC by high temperature (400 °C–900 °C) etching with NaOH solution (Yang

et al 2017). Electrochemical results have produced energy densities of 42 W h kg^{-1} at a power density of 30 kW kg^{-1} (Yang *et al* 2017). Pyrolysis and chlorination of xerogel based SiOC-precursor derived carbons for supercapacitor applications has been probed by Meier *et al* (2014). They have been able to obtain carbon samples with porosities greater than 200 m^2 g^{-1}, and specific capacitances of up to 110 F g^{-1} have been obtained in organic electrolytes (Meier *et al* 2014).

Table 2 summarizes some of the important results of using PDCs as electrodes in for supercapacitor applications, along with their pyrolysis temperatures.

5. Outlook, drawbacks and general prospects of PDCs as electrochemical energy storage devices

PDCs are starting to receive increasing attention because of their superior properties and high theoretical capacities. However, several challenges persist that must be overcome for widespread deployment of PDCs as electrodes in energy storage systems—both batteries and supercapacitors. The relatively high cost of the pre-ceramic polymer precursor is an important concern; this cost is often more than that of battery-grade graphite, which is the negative electrode material in commercial LIB systems. Secondly, the processing temperature of PDCs is high (~1000 °C), which makes their fabrication an energy intensive process (Mera *et al* 2010). Thirdly, a high first cycle capacity loss i.e. low first cycle coulombic efficiency is often a concern. Finally, PDCs also show a voltage hysteresis, indicating energy inefficiency (Dibandjo *et al* 2012).

The outlook ahead lies in overcoming these obstacles, and considerable research is being pursued to achieve these objectives. PDCs in general provide high capacities— about ten times higher than graphite, if cycled at high current densities—and this can negate the higher cost over graphite to a large extent (Ahn and Raj 2011). Fine tuning the synthesis so as to obtain the right phase/composition (as demonstrated in figure 4) will lead to higher capacity and lower first cycle losses (Dibandjo *et al* 2012). Preliminary studies suggest large hysteresis losses can be reduced to some degree by cycling at low currents, but research in this area is still developing (Ahn and Raj 2010).

6. Conclusion

PDCs are a unique group of compounds whose properties can be suitably tailored based on composition of the pre-ceramic polymer and processing parameters (temperature, gas environment, etc). As such, these materials offer a wide range of parameters that can be engineered to obtain electrochemical properties desirable for metal–ion batteries or supercapacitor systems. For example, negligible capacity fading at high current for LIBs is attained in PDCs that are carbon-rich and contain silicon mixed bonds; large sized Na^+ ions could be accommodated in low density amorphous PDCs via adsorption in micro-/nanovoids and the disordered carbon phase; and ultra-fast charge and discharge is demonstrated in carbon-rich PDCs and nanocomposites in aqueous supercapacitor devices. In addition, there seems to be progress being made gradually in studying PDC-derived thin films and nanomaterials, which will provide more enhanced properties than at the bulk scale.

As more diverse ranges of PDC and PDC-based composite materials are starting to emerge, their application as battery and supercapacitor electrodes will further our understanding of important phenomenological information about reaction mechanisms. Also, a greater control over the phase distribution during PDC synthesis will result in efficient utilization of the precursors so that maximum energy density can be obtained. It is hoped that this novel materials, with their suitable properties, will find applications in electrochemical energy storage in the years to come.

Acknowledgment

Financially support from National Science Foundation Grant Nos. 1335862, 1743701, and 1454151 is gratefully acknowledged.

ORCID iDs

Gurpreet Singh https://orcid.org/0000-0002-1719-9525

References

Abass M A, Syed A A, Gervais C and Singh G 2017 Synthesis and electrochemical performance of a polymer-derived silicon oxycarbide/boron nitride nanotube composite *RSC Adv.* **7** 21578–84

Ahn D and Raj R 2010 Thermodynamic measurements pertaining to the hysteretic intercalation of lithium in polymer-derived silicon oxycarbide *J. Power Sources* **195** 3900–6

Ahn D and Raj R 2011 Cyclic stability and C-rate performance of amorphous silicon and carbon based anodes for electrochemical storage of lithium *J. Power Sources* **196** 2179–86

Ahn D, Lee M and Shah S R 2010 Electrode material, lithium-ion battery and method thereof *US Patent Application* 12/483.631

An S J, Li J, Daniel C, Mohanty D, Nagpure S and Wood D L III 2016 The state of understanding of the lithium-ion-battery graphite solid electrolyte interphase (SEI) and its relationship to formation cycling *Carbon* **105** 52–76

Arbizzani C, Gabrielli G and Mastragostino M 2011 Thermal stability and flammability of electrolytes for lithium-ion batteries *J. Power Sources* **196** 4801–5

Baggetto L, Hah H-Y, Jumas J-C, Johnson C E, Johnson J A, Keume J K, Bridges C A and Veith G M 2014 The reaction mechanism of SnSb and Sb thin film anodes for Na-ion batteries studied by x-ray diffraction 119Sn and 121Sb Mössbauer spectroscopies *J. Power Sources* **267** 329–36

Baldus P, Jansen M and Sporn D 1999 Ceramic fibers for matrix composites in high-temperature engine applications *Science* **285** 699–703

Barré A, deguilhem B, Grolleau S, Gérard M, Suard F and Riu D 2013 A review on lithium-ion battery ageing mechanisms and estimations for automotive applications *J. Power Sources* **241** 680–9

Bedekar V, Singh G, Mahajan R L and Priya S 2010 Synthesis and microstructural characterization of barium titanate nanoparticles decorated SiCN-MWCNT nanotubes—'nanoNecklace' *Ferroelectr. Lett.* **36** 133–40
Bernard S and Miele P 2014 Ordered mesoporous polymer-derived ceramics and their processing into hierarchically porous boron nitride and silicoboron carbonitride monoliths *New J. Chem.* **38** 1923–31
Bernardo E, Fiocco L, Parcianello G, Storti E and Colombo P 2014 Advanced ceramics from preceramic polymers modified at the nano-scale: a review *Materials* **7** 1927–56
Bhandavat R and Singh G 2012a Improved electrochemical capacity of precursor-derived Si(B)CN-carbon nanotube composite as Li-ion battery anode *Appl. Mater. Interfaces* **4** 5092–7
Bhandavat R and Singh G 2012b Synthesis, characterization, and high temperature stability of Si(B)CN-coated carbon nanotubes using a boron-modified poly(ureamethylvinyl)silazane chemistry *J. Am. Ceram. Soc.* **95** 1536–43
Bhandavat R, Kuhn W, Mansfield E, Lehman J and Singh G 2012a Synthesis of polymer-derived ceramic Si(B)CN-carbon nanotube composite by microwave-induced interfacial polarization *ACS Appl. Mater. Interfaces* **4** 11–6
Bhandavat R, Pei Z and Singh G 2012b Polymer-derived ceramics as anode material for rechargeable Li-ion batteries: a review *Nanomater. Energy* **1** 324–37
Bhattacharyya R, Key B, Chen H, Best A S, Hollenkamp A F and Grey C P 2010 *In situ* NMR observation of the formation of metallic lithium microstructures in lithium batteries *Nat. Mater.* **9** 504–10
Bill J and Heimann D 1996 Polymer-derived ceramic coatings on C/C–SiC composites *J. Eur. Ceram. Soc.* **16** 1115–20
Blomgren G E 2017 The development and future of lithium ion batteries *J. Electrochem. Soc.* **164** A5019–25
Bourderau S, Brousse T and Schleich D M 1999 Amorphous silicon as a possible anode material for Li-ion batteries *J. Power Sources* **81–2** 233–6
Bruce P G, Scrosati B and Tarascon J-M 2008 Nanomaterials for rechargeable lithium batteries *Angew. Chem.* **48** 2930–46
Chan C K, Peng H, Liu G, Mcilwrath K, Zhang X F, Huggins R A and Cui Y 2008 High-performance lithium battery anodes using silicon nanowires *Nat. Nanotechnol.* **3** 31–5
Chandra C and Kim J 2018 Silicon oxycarbide produced from silicone oil for high-performance anode material in sodium ion batteries *Chem. Eng. J.* **338** 126–36
Chen K and Xue D 2016 Materials chemistry toward electrochemical energy storage *J. Mater. Chem.* A **4** 7522–37
Colombo P, Gambaryan-Roisman T, Scheffler M, Buhler P and Greil P 2001 Conductive ceramic foams from preceramic polymers *J. Am. Ceram. Soc.* **84** 2265–8
Colombo P, Mera G, Riedel R and Sorarù G D 2010 Polymer-derived ceramics: 40 years of research and innovation in advanced ceramics *J. Am. Ceram. Soc.* **93** 1805–37
Cordelair J and Greil P 2000 Electrical conductivity measurements as a microprobe for structure transitions in polysiloxane derived Si ± O ± C ceramics *J. Eur. Ceram. Soc.* **20** 1947–57
Cross T J, Raj R, Prasad S V and Tallant D R 2006 Synthesis and tribological behavior of silicon oxycarbonitride thin films derived from poly(urea)methyl vinyl silazane *Int. J. Appl. Ceram. Technol.* **3** 113–26
Dahn J R, Zheng T, Liu Y and Xue J S 1995 Mechanisms for lithium insertion in carbonaceous materials *Science* **270** 590–3
David L, Asok D and Singh G 2014 Synthesis and extreme rate capability of Si−Al−C−N functionalized carbon nanotube spray-on coatings as Li-ion battery electrode *Appl. Mater. Interfaces* **6** 16056–64
David L, Bhandavat R, Barrera U and Singh G 2016a Silicon oxycarbide glass-graphene composite paper electrode for long-cycle lithium-ion batteries *Nat. Commun.* **7** 1–10
David L, Shareef K M, Abass M A and Singh G 2016b Three-dimensional polymer derived ceramic/graphene paper as a Li-ion battery and supercapacitor electrode *RSC Adv.* **6** 53894–902
Dibandjo P, Graczyk-Zajac M, Riedel R, Pradeep V S and Soraru G D 2012 Lithium insertion into dense and porous carbon-rich polymer-derived SiOC ceramics *J. Eur. Ceram. Soc.* **32** 2495–503
Ellis B L and Nazar L F 2012 Sodium and sodium-ion energy storage batteries *Curr. Opin. Solid State Mater. Sci.* **16** 168–77
Erb D and Lu K 2018 Influence of vinyl bonds from PDMS on the pore structure of polymerderived ceramics *Mater. Chem. Phys.* **209** 217–26
Feng Y 2010 Electrochemical properties of heat-treated polymer-derived SiCN anode for lithium ion batteries *Electrochem. Acta* **55** 5860–6
Feng Y, Dou S, Wei Y, Zhang Y, Song X, Li X and Battaglia V S 2017 Preparation and capacity-fading investigation of polymer-derived silicon carbonitride anode for lithium-ion battery *ACS Omega* **2** 8075–85
Feng Y, Feng N, Wei Y and Bai Y 2014 Preparation and improved electrochemical performance of SiCN-graphene composite derived from poly(silylcarbondiimide) as Li-ion battery anodes *J. Mater. Chem.* A **2** 4168–77
Fukui H, Harimoto Y, Akasaka M and Eguchi K 2014 Lithium species in electrochemically lithiated and delithiated silicon oxycarbides *ACS Appl. Mater. Interfaces* **6** 12827–36
Fukui H, Nakata N, Dokko K, Takemura B, Ohsuka H, Hino T and Kanamura K 2011a Lithiation and delithiation of silicon oxycarbide single particles with a unique microstructure *ACS Appl. Mater. Interfaces* **3** 2318–22
Fukui H, Ohsuka H, Hino T and Kanamura K 2009 Preparation of microporous Si–O–C composite material and its lithium storage capability *Chem. Lett.* **38** 86–7
Fukui H, Ohsuka H, Hino T and Kanamura K 2010 A Si–O–C composite anode: high capability and proposed mechanism of lithium storage associated with microstructural characteristics *ACS Appl. Mater. Interfaces* **2** 998–1008
Fukui H, Ohsuka H, Hino T and Kanamura K 2011b Influence of polystyrene/phenyl substituents in precursors on microstructures of Si–O–C composite anodes for lithium-ion batteries *J. Power Sources* **196** 371–8
Fukui H, Ohsuka H, Hino T and Kanamura K 2011c Polysilane/acenaphthylene blends toward Si–O–C composite anodes for rechargeable lithium-ion batteries *J. Electrochem. Soc.* **158** A550–5
Goodenough J B and Park K-S 2013 The Li-ion rechargeable battery: a perspective *J. Am. Chem. Soc.* **135** 1167–76
Graczyk-Zajac M, Fasel C and Riedel R 2011 Polymer-derived-SiCN ceramic/graphite composite as anode material with enhanced rate capability for lithium ion batteries *J. Power Sources* **196** 6412–8
Graczyk-Zajac M, Mera G, Kaspar J and Riedel R 2010 Electrochemical studies of carbon-rich polymer-derived SiCN ceramics as anode materials for lithium-ion batteries *J. Eur. Ceram. Soc.* **30** 3235–43
Graczyk-Zajac M, Toma L, Fasel C and Riedel R 2012 Carbon-rich SiOC anodes for lithium-ion batteries: part I. Influence of material UV-pre-treatment on high power properties *Solid State Ion.* **225** 522–6
Greil P 1998 Near net shape manufacturing of polymer derived ceramics *J. Eur. Ceram. Soc.* **18** 1905–14
Guron M M, Kim M J and Sneddon L G 2008 A simple polymeric precursor strategy for the syntheses of complex zirconium and hafnium-based ultra high-temperature silicon-carbide composite ceramics *J. Am. Ceram. Soc.* **91** 1412–5
Halim M, Liu G, Ardhi R E A, Hudaya C, Wijaya O, Lee S-H, Kim A-Y and Lee J K 2017 Pseudocapacitive characteristics of

low-carbon silicon oxycarbide for lithium-ion capacitors *Appl. Mater. Interfaces* **9** 20566–76
Haluschka C, Engel C and Riedel R 2000 Silicon carbonitride ceramics derived from polysilazanes. Part II. Investigation of electrical properties *J. Eur. Ceram. Soc.* **20** 1365–74
Hsieh Y-C, Lee K-T, Lin Y-P, Wu N-L and Donne S W 2008 Investigation on capacity fading of aqueous $MnO_2 \cdot nH_2O$ electrochemical capacitor *J. Power Sources* **177** 660–4
Ionescu E, Kleebe H-J and Riedel R 2012 Silicon-containing polymer-derived ceramic nanocomposites (PDC-NCs): preparative approaches and properties *Chem. Soc. Rev.* **41** 5032–52
Jalowiecki A, Bill J and Aldinger F 1996 Interface characterization of nanosized B-doped Si_3N_4/SiC ceramics *Composites* A **27A** 717–21
Ji F, Li Y-L, Feng J-M, Su D, Wen Y-Y, Feng Y and Hou F 2009 Electrochemical performance of graphene nanosheets and ceramic composites as anodes for lithium batteries *J. Mater. Chem.* **19** 9063–7
Jiang J, Li Y, Liu J, Huang X, Yuan C and Lou X W D 2012 Recent advances in metal oxide-based electrode architecture design for electrochemical energy storage *Adv. Mater.* **24** 5166–80
Kaspar J, Graczyk-Zajac M and Riedel R 2012 Carbon-rich SiOC anodes for lithium-ion batteries: part II. Role of thermal cross-linking *Solid State Ion.* **225** 527–31
Kaspar J, Graczyk-Zajac M and Riedel R 2013 Lithium insertion into carbon-rich SiOC ceramics: influence of pyrolysis temperature on electrochemical properties *J. Power Sources* **244** 450–5
Kaspar J, Graczyk-Zajac M, Choudhury S and Riedel R 2016a Impact of the electrical conductivity on the lithium capacity of polymer-derived silicon oxycarbide (SiOC) ceramics *Electrochem. Acta* **216** 196–202
Kaspar J, Graczyk-Zajac M, Lauterbach S, Kleebe H-J and Riedel R 2014 Silicon oxycarbide/nano-silicon composite anodes for Li-ion batteries: considerable influence of nano-crystalline versus nano-amorphous silicon embedment on the electrochemical properties *J. Power Sources* **269** 164–72
Kaspar J, Mera G, Nowak A P, Graczyk-Zajac M and Riedel R 2010 Electrochemical study of lithium insertion into carbon-rich polymer-derived silicon carbonitride ceramics *Electrochem. Acta* **56** 174–82
Kaspar J, Storch M, Schitco C, Riedel R and Graczyk-Zajac M 2016b SiOC(N)/hard carbon composite anodes for Na-ion batteries: influence of morphology on the electrochemical properties *J. Electrochem. Soc.* **163** A156–62
Kaspar J 2014 Carbon-rich silicon oxycarbide (SiOC) and silicon oxycarbide/element (SiOC/X, X = Si, Sn) nano-composites as new anode materials for Li-ion battery application *PhD Thesis* Technische Universität Darmstadt
Kim M, Oh I and Kim J 2016a Carbonization temperature dependence of pore structure of silicon carbide spheres and their electrochemical capacitive properties as supercapacitors *Ceram. Int.* **42** 3947–58
Kim M, Oh I and Kim J 2016b Influence of surface oxygen functional group on the electrochemical behavior of porous silicon carbide based supercapacitor electrode *Electrochim. Acta* **196** 357–68
Kim T, Mo Y H, Nahm K S and Oh S M 2006 Carbon nanotubes (CNTs) as a buffer layer in silicon/CNTs composite electrodes for lithium secondary batteries *J. Power Sources* **162** 1275–81
Kleebe H J, Störmer H, Trassl S and Ziegler G 2001 Thermal stability of SiCN ceramics studied by spectroscopy and electron microscopy *Appl. Organometal. Chem.* **15** 858–66
Kolb R, Fasel C, Liebau-Kunzmann V and Riedel R 2006 SiCN/C-ceramic composite as anode material for lithium ion batteries *J. Eur. Ceram. Soc.* **26** 3903–8
Konno H, Morishita T, Sato S, Habazaki H and Inagaki M 2005 High-capacity negative electrode materials composed of Si–C–O glass-like compounds and exfoliated graphite for lithium ion battery *Carbon* **43** 1084–114
Kroll P 2003 Modelling and simulation of amorphous silicon oxycarbide *J. Mater. Chem.* **13** 1657–68
Kumar B V M and Kim Y-W 2010 Processing of polysiloxane-derived porous ceramics: a review *Sci. Technol. Adv. Mater.* **11** 044303
Kundu D, Talaie E, Duffort V and Nazar L F 2015 The emerging chemistry of sodium ion batteries for electrochemical energy storage *Angew. Chem.* **54** 3431–48
Landi B J, Dileo R A, Schauerman C M, Cress C D, Ganter M J and Raffaelle R P 2009 Multi-walled carbon nanotube paper anodes for lithium ion batteries *J. Nanosci. Nanotechnol.* **9** 3406–10
Lee S S, Lim Y J, Kim H, Kim J-K, Jung Y-G and Kim Y 2016 Electrochemical properties of a ceramic-polymer-composite-solid electrolyte for Li-ion batteries *Solid State Ion.* **284** 20–4
Lee Y, Lee K Y and Choi W 2017 One-pot synthesis of antimony-embedded silicon oxycarbide materials for high-performance sodium-ion batteries *Adv. Funct. Mater.* **27** 1702607–20
Lehman J H, Hurst K E, Singh G, Mansfield E, Perkins J D and Cromer C L 2010 Core–shell composite of SiCN and multiwalled carbon nanotubes from toluene dispersion *J. Mater. Sci.* **2010** 4251–4
Lei J-C, Zhang X and Zhou Z 2015 Recent advances in MXene: preparation properties and applications *Frontiers Phys.* **10** 276–86
Li Y *et al* 2014 One-dimensional SiOC/C composite nanofibers as binder-free anodes for lithium-ion batteries *J. Power Sources* **254** 33–8
Liebau-Kunzmann V, Fasel C, Kolb R and Riedel R 2006 Lithium containing silazanes as precursors for SiCN:Li ceramics—a potential material for electrochemical applications *J. Eur. Ceram. Soc.* **26** 3897–901
Liqun D, Qingsong M, Lin M and Zhaohui C 2015 Fabrication and electrochemical performance of nanoporous carbon derived from silicon oxycarbide *Microporous Mesoporous Mater.* **202** 97–105
Liu G, Kaspar J, Reinold L M, Graczyk-Zajac M and Riedel R 2013 Electrochemical performance of DVB-modified SiOC and SiCN polymer-derived negative electrodes for lithium-ion batteries *Electrochem. Acta* **106** 101–8
Liu X, Zheng M-C and Xie K 2011 Mechanism of lithium storage in Si–O–C composite anodes *J. Power Sources* **196** 10667–72
Liu X, Zheng M-C, Xie K and Liu J 2012a The relationship between the electrochemical performance and the composition of Si–O–C materials prepared from a phenyl-substituted polysiloxane utilizing various processing methods *Electrochem. Acta* **59** 304–9
Liu X-M, Huang Z D, Oh S W, Zhang B, Ma P-C, Yuen M M F and Kim J-K 2012b Carbon nanotube (CNT)-based composites as electrode material for rechargeable Li-ion batteries: a review *Compos. Sci. Technol.* **72** 121–44
Luo X, Wang J, Dooner M and Clarke J 2015 Overview of current development in electrical energy storage technologies and the application potential in power system operation *Appl. Energy* **137** 511–36
Mazo M A, Tamayo A and Rubio J 2016 Advanced silicon oxycarbide-carbon composites for high temperature resistant friction systems *J. Eur. Chem. Soc.* **36** 2443–52
Meier A, Weinberger M, Pinkert K, Oschatz M, Paasch S, Giebeler L, Althues H, Brunner E, Eckert J and Kaskel S 2014 Silicon oxycarbide-derived carbons from a polyphenylsilsequioxane precursor for supercapacitor applications *Microporous Mesoporous Mater.* **188** 140–8
Mera G, Navrotsky A, Sen S, Kleebe H-J and Riedel R 2013 Polymer-derived SiCN and SiOC ceramics—structure and energetics at the nanoscale *J. Mater. Chem.* A **1** 3826–36

Mera G, Riedel R, Poli F and Muller K 2009 Carbon-rich SiCN ceramics derived from phenyl-containing poly(silylcarbondiimides) *J. Eur. Ceram. Soc.* **29** 2873–83
Mera G, Tamayo A, Nguyen H, Sen S and Riedel R 2010 Nanodomain structure of carbon-rich silicon carbonitride polymer-derived ceramics *J. Am. Chem. Soc.* **93** 1169–75
Morcos R M, Mera G, Navrotsky A, Varga T, Riedel R, Poli F and Muller K 2008 Enthalpy of formation of carbon-rich polymer-derived amorphous SiCN ceramics *J. Am. Ceram. Soc.* **91** 3349–4
Mukherjee S, Schuppert N, Bates A, Jasinski J, Hong J-E, Choi M J and Park S 2017 An electrochemical and structural study of highly uniform tin oxide nanowires fabricated by a novel scalable solvoplasma technique as anode material for sodium ion batteries *J. Power Sources* **347** 201–9
Obrovac M N and Christensen L 2004 Structural changes in silicon anodes during lithium insertion/extraction *Electrochem. Solid State Lett.* **7** A93–6
Pradeep V S, Graczyk-Zajac M, Riedel R and Soraru G D 2014a New insights in to the lithium storage mechanism in polymer derived SiOC anode materials *Electrochem. Acta* **119** 78–85
Pradeep V S, Graczyk-Zajac M, Wilamowska W, Riedel R and Soraru G D 2014b Influence of pyrolysis atmosphere on the lithium storage properties of carbon-rich polymer derived SiOC ceramic anodes *Solid State Ion.* **262** 22–4
Reinold L M, Graczyk-Zajac M, Gao Y, Mera G and Riedel R 2013 Carbon-rich SiCN ceramics as high capacity/high stability anode material for lithium-ion batteries *J. Power Sources* **236** 224–9
Reinold L M, Yamada Y, Graczyk-Zajac M, Munakata H, Kanamura K and Riedel R 2015 The influence of the pyrolysis temperature on the electrochemical behavior of carbon-rich SiCN polymer-derived ceramics as anode materials in lithium-ion batteries *J. Power Sources* **282** 409–15
Riedel R, Mera G, Hauser R and Klonczynski A 2006 Silicon-based polymer-derived ceramics: synthesis properties and applications—a review *J. Ceram. Soc. Japan* **114** 425–44
Saha A and Raj R 2006 A model for the nanodomains in polymer-derived SiCO *J. Am. Ceram. Soc.* **89** 2188–95
Saint J, Morcrette M, Larcher D, Laffont L, Beattie S, Pérès J-P, Talaga D, Couzi M and Tarascon J-M 2007 Towards a fundamental understanding of the improved electrochemical performance of silicon–carbon composites *Adv. Funct. Mater.* **17** 1765–74
Sawicki M and Shaw L L 2015 Advances and challenges of sodium ion batteries as post lithium ion batteries *RSC Adv.* **5** 53129–54
Scrosati B and Garche J 2010 Lithium batteries: status prospects and future *J. Power Sources* **195** 2419–30
Scrosati B, Hassoun J and Sun Y-K 2011 Lithium-ion batteries. A look into the future *Energy Environ. Sci.* **4** 3287–95
Seko S, Nara H, Jeong M, Yokoshim T, Momma T and Osaka T 2017 Carbonate-based additive for improvement of cycle durability of electrodeposited Si–O–C composite anode in glyme-based ionic liquid electrolyte for use in lithium secondary batteries *Electrochem. Acta* **243** 65–71
Shah S R and Raj R 2002 Mechanical properties of a fully dense polymer derived ceramic made by a novel pressure casting process *Acta Mater.* **50** 4093–103
Shen J and Raj R 2011 Silicon-oxycarbide based thin film anodes for lithium ion batteries *J. Power Sources* **196** 5945–50
Shen J, Ahn D and Raj R 2011 C-rate performance of silicon oxycarbide anodes for Li+ batteries enhanced by carbon nanotubes *J. Power Sources* **196** 2875–8
Singh G, Priya S, Hossu M R, Shah S R, Grover S, Koymen A R and Mahajan R L 2009 Synthesis, electrical and magnetic characterization of core–shell silicon carbo-nitride coated carbon nanotubes *Mater. Lett.* **63** 2435–8
Slater M D, Kim D, Lee E and Johnson C S 2013 Sodium-ion batteries *Adv. Funct. Mater.* **23** 947–58
Smith A J, Burns J C, Trussler S and Dahn J R 2010 Precision measurements of the coulombic efficiency of lithium-ion batteries and of electrode materials for lithium-ion batteries *J. Electrochem. Soc.* **157** A196–202
Soraru G D and Modena S 2002 Chemical durability of silicon oxycarbide glasses *J. Am. Ceram. Soc.* **85** 1529–36
Stevens D A and Dahn J R 2000 High capacity anode materials for rechargeable sodium-ion batteries *J. Electrochem. Soc.* **147** 1271–3
Storch M, Vrankovic D, Graczyk-Zajac M and Riedel R 2018 The influence of pyrolysis temperature on the electrochemical behavior of porous carbon-rich SiCN polymer-derived ceramics *Solid State Ion.* **315** 59–64
Stormer H, Kleebe H-J and Ziegler G 2007 Metastable SiCN glass matrices studied by energy-filtered electron diffraction pattern analysis *J. Non-Cryst. Solids* **353** 2867–77
Su D, Li Y L, Feng Y and Jin J 2009 Electrochemical properties of polymer-derived SiCN materials as the anode in lithium ion batteries *J. Am. Ceram. Soc.* **92** 2962–8
Sun H and Zhao K 2017 Atomistic origins of high capacity and high structural stability of polymer-derived SiOC anode materials *ACS Appl. Mater. Interfaces* **9** 35001–9
Tolosa A, Krüner B, Jackel N, Aslan M, Vakifahmetoglu C and Presser V 2016 Electrospinning and electrospraying of silicon oxycarbide-derived nanoporous carbon for supercapacitor electrodes *J. Power Sources* **313** 178–88
Vakifahmetoglu C, Zeydanli D and Colombo P 2016 Porous polymer derived ceramics *Mater. Sci. Eng.* R **106** 1–30
Vrankovic D, Graczyk-Zajac M, Kalcher C, Rohrer J, Becker M, Stabler C, Trykowski G, Albe K and Riedel R 2017 Highly porous silicon embedded in a ceramic matrix: a stable high-capacity electrode for Li-ion batteries *Acs Nano* **11** 11409–16
Wang S, Hu X and Dai Y 2017 Preparation and electrochemical performance of polymer-derived SiBCN-graphene composite as anode material for lithium ion batteries *Cheram. Int.* **43** 1210–6
Wilamowska M, Graczyk-Zajac M and Riedel R 2013 Composite materials based on polymer-derived SiCN ceramic and disordered hard carbons as anodes for lithium-ion batteries *J. Power Sources* **244** 80–6
Wilson A M, Reimers J N, Fuller E W and Dahn J R 1994 Lithium insertion in pyrolyzed siloxane polymers *Solid State Ion.* **74** 249–54
Winter M, Besenhard J O, Spahr M E and Novak P 1998 Insertion electrode materials for rechargeable lithium batteries *Adv. Mater.* **10** 725–63
Xia K, Wu Z, Xuan C, Xiao W, Wang J and Wang D 2017 Effect of KOH etching on the structure and electrochemical performance of SiOC anodes for lithium-ion batteries *Electrochem. Acta* **245** 287–95
Xing W B, Wilson A M, Eguchi K, Zank G and Dahn J R 1997 Pyrolyzed polysiloxanes for use as anode materials in lithium-ion batteries *J. Electrochem. Soc.* **144** 2410–6
Xua J, Deshpande R D, Pan J, Cheng Y-T and Battaglia V S 2015 Electrode side reactions capacity loss and mechanical degradation in lithium-ion batteries *J. Electrochem. Soc.* **162** A2026–35
Yabuuchi N, Kubota K, Dahbi M and Komaba S 2014 Research development on sodium-ion batteries *Chem. Rev.* **114** 11636–82
Yajima S, Hayashi J, Omori M and Okamura K 1976 Development of a silicon carbide fibre with high tensile strength *Nature* **261** 683–5

Yang J, Wu H, Zhu M, Ren W, Lin Y, Chen H and Pan F 2017 Optimized mesopores enabling enhanced rate performance in novel ultrahigh surface area meso-/microporous carbon for supercapacitors *Nano Energy* **33** 453–61

Yu C, Ganapathy S, Eck E R H V, Wang H, Basak S, Li Z and Wagemaker M 2017 Accessing the bottleneck in all-solid state batteries, lithium-ion transport over the solid-electrolyte-electrode interface *Nat. Commun.* **8** 1–9

Yu L and Raj R 2015 On the thermodynamically stable amorphous phase of polymer-derived silicon oxycarbide *Sci. Rep.* **5** 14550

Yu X and Manthiram A 2018 Electrode–electrolyte interfaces in lithium-based batteries *Energy Environ. Sci.* **11** 527–43

Yuan Y, Amine K, Lu J and Shahbazian-Yassar R 2017 Understanding materials challenges for rechargeable ion batteries with *in situ* transmission electron microscopy *Nat. Commun.* **8** 1–14

Zhang W-J 2011 A review of the electrochemical performance of alloy anodes for lithium-ion batteries *J. Power Sources* **196** 13–24

Zhao C and Zheng W 2015 A review for aqueous electrochemical supercapacitors *Frontiers Energy Res.* **3** 1–11